Wavelength-selective vibrationally excited photodesorption with tunable IR sources

2006 J. Phys.: Condens. Matter 18 S1357

(http://iopscience.iop.org/0953-8984/18/30/S02)

INSTITUTE OF PHYSICS PUBLISHING JOURNAL OF PHYSICS: CONDENSED MATTER

J. Phys.: Condens. Matter **18** (2006) S1357–S1387 doi:10.1088/0953-8984/18/30/S02

Wavelength-selective vibrationally excited photodesorption with tunable IR sources

C Focsa[1,3], C Mihesan[1,2], M Ziskind[1], B Chazallon[1], E Therssen[2], P Desgroux[2] and J L Destombes[1]

[1] Laboratoire de Physique des Lasers, Atomes et Molécules (UMR 8523), Centre d'Etudes et de Recherches Lasers et Applications (FR CNRS 2416), Université de Lille 1, 59655 Villeneuve d'Ascq cedex, France

[2] Laboratoire de Physico-Chimie des Processus de Combustion et de l'Atmosphère (UMR 8522), Centre d'Etudes et de Recherches Lasers et Applications (FR CNRS 2416), Université de Lille 1, 59655 Villeneuve d'Ascq cedex, France

E-mail: focsa@phlam.univ-lille1.fr

Received 3 January 2006
Published 14 July 2006
Online at stacks.iop.org/JPhysCM/18/S1357

Abstract

We present an overview of IR laser resonant desorption (LRD) studies with special focus on recent developments by our group. The resonant character of the laser desorption process mediated by O–H, C–H, and N–H vibrational modes in the 3 μm spectral range has been investigated on ice, PAH and ammonia samples, respectively. The desorption of cryogenic binary mixtures is also presented. An interesting wavelength-selective effect has been found by comparative IR/visible or IR/IR irradiation studies. At higher fluences and/or analyte concentration values a loss of selectivity occurs, with extensive co-desorption of both components and clustering phenomena. Insights on the desorption mechanisms involved are presented through an ejecta velocity distribution study. Finally, possible technological and analytical potentialities are discussed, in the fields of IR-MALDI, LRD depth profiling, pulsed laser cleaning and selective analysis of complex samples.

(Some figures in this article are in colour only in the electronic version)

1. Introduction

The development during the last decades of new techniques like matrix-assisted laser desorption and ionization (MALDI) [1, 2], laser resonant desorption (LRD) depth profiling [3, 4] or matrix-assisted pulsed laser evaporation (MAPLE) [5], led to an increased interest in the study of the photo-excited desorption of condensed matter. To optimally exploit the

[3] Author to whom any correspondence should be addressed.

analytical and technological capabilities of these techniques, a better understanding of the complex laser–sample interaction fundamentals, in terms of optical and thermal processes involved, wavelength and fluence dependence, or ejection products, seems therefore necessary (see, e.g., [6, 7]).

Compared to the extensively studied DIET (desorption induced by electronic transitions) processes in the UV range, IR vibrationally stimulated photodesorption is less documented. However, the feasibility of desorption through resonant coupling of the energy in vibration modes of adsorbates had been demonstrated in the early 1980s using CO_2 lasers in the 10 μm spectral range [8–13] (see also [14] for a review of these early works). The further development of these studies in other IR regions has been partly limited by the lack of broadly tunable intense pulsed IR laser sources. The recent availability of free electron lasers (FELs) and optical parametric oscillators (OPOs) offered the opportunity to fill this gap. While the CO_2 lasers had limited tunability, the new sources have given access to a wide IR spectral range, covering different vibration modes.

These new developments have also been triggered by the emergence of the IR-MALDI technique, which especially uses the O–H, N–H, C–H or C = O stretching modes (naturally present in organic matrices) as energy coupling channels to promote desorption and ionization of biological interest analytes. A relatively important number of papers [15–28] have tested the efficiency of different IR wavelengths for various MALDI matrices, especially in the 2.7–4 and 5–6 μm spectral ranges (see [28] for a recent review of this field). In another analytical direction, IR laser resonant desorption has been extensively used by George's group [2, 3, 29, 30] for laboratory experiments on physical processes involving interaction between ice samples and atmospheric trace gases. The importance of the irradiation wavelength for the IR desorption of different materials has also been studied, for example on calcite [31, 32], fused silica [32] or diamond [33]. In the pulsed laser deposition of polymers, the IR approach has been proven to present particular interest [34], as the tunable IR laser can resonantly excite the polymer to a vibrationally excited ground electronic state without accessing the photochemically active excited electronic states. Finally, IR laser radiation interaction with water in living tissues is another subject of interest: the short optical penetration depth ($\sim$1 μm) in water at 2.94 μm (Er:YAG lasers) leaves thin zones of thermal collateral damage which is a desirable attribute for laser surgery [35, 36].

The main concern of this paper is the resonant character of the desorption process, i.e., the correlation between the desorption yield and the optical absorption profiles. In this frame, relatively few fundamental results have been reported to date: in addition to the MALDI investigations [17–19, 21–23, 25, 28], we can cite the studies on the O–H [37, 38] C–H [39–41] or N–H [42, 43] stretching modes. The C = O stretching mode around 6 μm has also been addressed in the MALDI field [17]. Finally, in a fundamental FEL study, Redlich *et al* [44] revealed the exact match between the desorption yields and the absorption bands for the ν_1 (symmetric stretching, 1293 cm^{-1}) and ν_2 (bending, 589 cm^{-1}) of N_2O adsorbed on NaCl (100).

We have developed in Lille an experimental set-up based on the use of a ns $LiNbO_3$ tunable optical parametric oscillator (OPO) in the 2.7–4 μm range. This set-up was initially dedicated to the study of ice-based samples of environmental and/or biological interest through O–H resonant coupling of energy [38, 45–48]. Recently we have extended these studies to the C–H [40, 41] and N–H stretching modes situated in the same spectral region.

This paper presents an overview of IR laser resonant desorption studies, with particular focus on the work carried out in our group. Investigations on pure samples are presented in the first part, followed by studies on cryogenic binary mixtures, where an interesting wavelength-selective desorption effect is evidenced. Some insights on the mechanisms involved are given

through the study of the velocity distribution of the ejecta. Finally, possible analytical and technological application are discussed, in the fields of IR-MALDI, IR-LRD depth profiling, pulsed laser cleaning, or selective analysis of complex samples.

2. Experimental details

Our experimental approach has been described in detail in several papers [38, 40, 41, 45–51]. It is based on the coupling of three techniques.

(1) IR laser resonant desorption of the condensed phase with a tunable (2.7–4 μm) optical parametric oscillator (Euroscan, Belgium) based on a $LiNbO_3$ non-linear crystal placed in a single-resonant planar cavity. The OPO idler wavelength is varied by changing the crystal phase matching angle with respect to the pump beam (10 ns Nd:YAG, 1064 nm, Quantel Brillant). The OPO idler energy is monitored by a pyroelectric detector (Oriel); the maximum energy available (at the sample) is $\sim$3 mJ/pulse, obtained with $\sim$160 mJ/pulse pump energy. For some specific experiments, the second harmonic (532 nm) of the YAG laser can be used as desorption beam (see below).
(2) UV multi-photon ionization of the ejecta by using the fourth harmonic (266 nm) of another 10 ns Nd:YAG laser (Continuum Powerlite 8010). The second harmonic of this laser can be used to pump a tunable dye-laser (Continuum ND6000). The visible beam obtained is then doubled and/or mixed with 1.064 μm radiation in non-linear crystals to obtain continuously tunable UV radiation down to 225 nm. This radiation can serve to achieve resonance-enhanced multi-photon ionization (REMPI).
(3) Time-of-flight mass spectrometry (TOF-MS) for the mass separation of the ionized particles.

Figure 1 presents a schematic view of the experimental set-up. It is composed basically of two vacuum chambers separated by a gate valve. The samples can be prepared *in situ* in the first (synthesis/preparation) chamber by gas phase deposition on different substrates (Cu, sapphire, etc) placed on a temperature-regulated cold finger. This latter is cooled by a liquid nitrogen flow and heated by a resistor to reach a given temperature in the range 90–320 K. For some studies, samples prepared *ex situ* can be used: e.g., frozen aqueous solutions or ice single crystals prepared in a cold chamber by Bridgman [52] or Petrenko [53] methods. In this case, a home-made vacuum interlock is used to avoid frost formation at the sample surface during transfer.

A typical residual vacuum of 10^{-8} Torr is attained in the synthesis/preparation chamber by using a turbo-molecular pump (Varian Turbo-V250). The composition of the gas phase in this chamber is monitored by a quadrupole mass spectrometer (Pfeiffer PRISMA 200) and regulated by a flow/pressure controller (Pfeiffer RVC300) which controls the opening of two needle valves (one for H_2O and one for the doping gas, in the case of structured samples used for diffusion studies). An interferometric method is used for the on-line control of the thickness of the deposited films. A chopper modulated (1250 Hz) He/Ne laser (632.8 nm) is injected in a monomode optical fibre introduced in the vacuum chamber by a special feedthrough. A collimating lens and a polarizer are placed at the sample end of the fibre, giving a $\sim$1 mm diameter spot on the sample surface. The time evolution of the interference fringes induced by the sample thickness variation is recorded by a photodiode, and the signal is demodulated by a lock-in amplifier and recorded on a digital scope.

Once the preparation of the sample is finished, the synthesis chamber is evacuated and the gate valve is opened for access to the analysis chamber (reflectron time-of-flight mass spectrometer, RM Jordan, Inc.). The analysis chamber has a lower residual vacuum

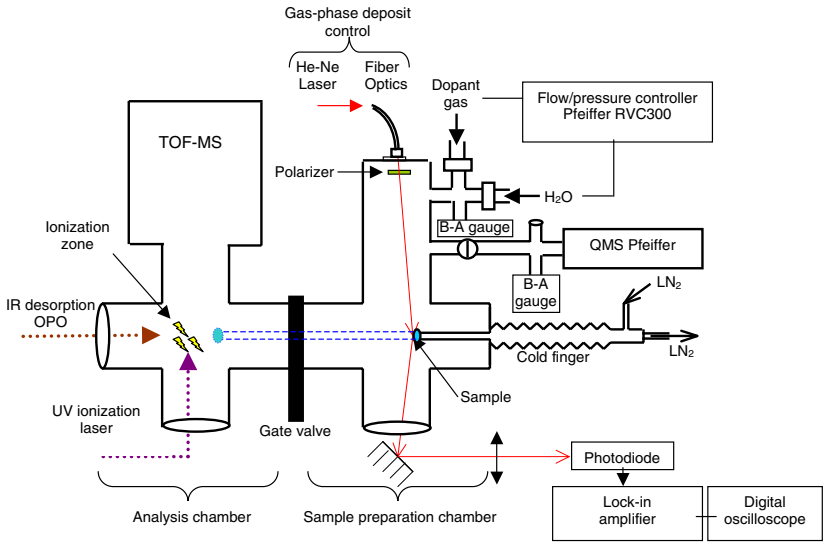

Figure 1. Schematic view of the experimental set-up.

($<10^{-9}$ Torr), obtained by using two turbo-molecular pumps (Varian Turbo-V 250 and 300 HT). The sample mounted on the cold finger is moved into the analysis chamber to ∼1 cm distance from the edge of the extraction (vertical) plates of the mass spectrometer. The desorption laser beam enters the analysis chamber through a sapphire window, then is focused by a $f = 15$ cm CaF_2 lens and passes horizontally between the extraction plates to irradiate the sample at normal incidence with 0.3–1 mm typical beam diameter at the sample surface.

The horizontal desorption plume (perpendicular to the sample surface) is intercepted in the central region between the extraction plates (i.e., at $\Delta z = 35$ cm from the sample surface) by the vertical beam of the UV ionization laser, focused (∼100 μm diameter beam) with a $f = 25$ cm quartz lens. The time delay between the ns desorption and ionization pulses is controlled by a delay/pulse generator (DG 535, Stanford Research System) and by a home-made timing circuit. The ions created are accelerated (3000 V) on the direction orthogonal to the two mentioned above and, after passing an XY deflector, an Einsel lens, the first free flight region (1 m long), the reflectron and the second free flight region (0.72 m), are detected by a pair of 1″ multi-channel plates (Hamamatsu) mounted in 'chevron' configuration. The transient signals are recorded by a 500 MHz digital oscilloscope (LeCroy AM 9350) and transferred to a PC through a GPIB interface for further treatment/storage using home-made software in a Labview (National Instruments) environment.

3. Resonant desorption of pure samples

3.1. O–H stretching

3.1.1. Resonant character of the desorption process. We investigated the resonant character of the desorption process promoted by the O–H stretching on pure H_2O ice samples [38]. This study is motivated by the high current interest in developing new sensitive, spatially resolved laser techniques to investigate fundamental processes at the surface/in the volume of this solid. Indeed, water ice plays a key role in many natural processes, from the Earth's surface and atmosphere (e.g., activation of chlorine at the surface of ice in polar stratospheric clouds,

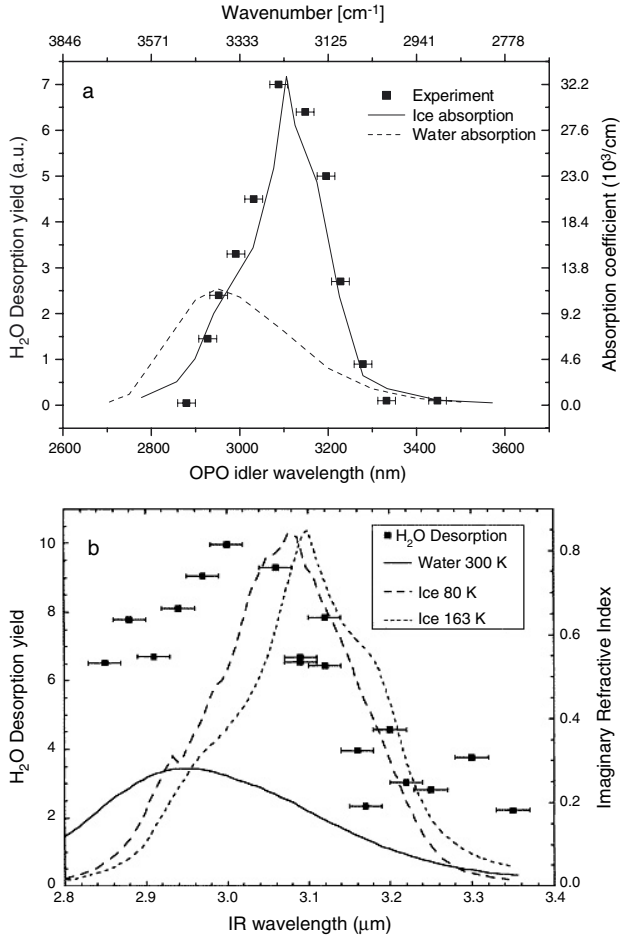

Figure 2. (a) Laser resonant desorption spectrum of ice obtained using a $LiNbO_3$ ns OPO: desorption yields (squares) are compared with the optical absorption spectra of ice ($T = 100$ K, solid line) and liquid water (dashed line). Reproduced with permission from [38]. (b) H_2O desorption yield (solid squares) from a 5 μm thick ice film at 110 K obtained with a free electron laser [37]. The imaginary index of refraction of amorphous ice deposited at 80 K (dashed line), polycrystalline ice deposited at 163 K (dotted line), and liquid water at 300 K (solid line) are also shown for comparison. Reproduced with permission from [37].

leading to the depletion of the ozone layer [54]) up to planetary and cometary material as well as interstellar grains [52, 55]. Moreover, water is the usual environment for living cells: cryogenic H_2O-based samples are therefore expected to be the first natural choice in efforts to develop new approaches for biology and medicine, with less or no external addition to the studied object. One example is the IR-MALDI technique using ice as the matrix (see below).

Ice samples (10–100 μm thick) were prepared by vapour deposition at constant pressure on a temperature-regulated cold finger (see [38] for details). In order to test the resonant character of the laser desorption mechanism, the OPO idler wavelength was varied in the 2.8–3.5 μm spectral range, by adjusting the phase-matching angle of the $LiNbO_3$ crystal. Desorption yields were recorded at 12 individual wavelengths in this spectral range, by averaging 20 successive laser shots ($\sim$1.5 mJ/pulse) hitting the same sample spot. The results are displayed

in figure 2(a), together with the optical absorption spectra of ice at 100 K (solid line) and liquid water (dashed line) [56, 57]. One can see that the experimental results exactly fit the ice absorption coefficient curve, and the desorption efficiency peak occurs at $\lambda \approx 3.1$ μm, in excellent agreement with the maximum of the optical absorption coefficient of ice.

These results contrast with those obtained by Krasnopoler and George [37] when using an FEL for the resonant desorption of ice. They found a desorption efficiency peak at $\lambda = 3.0$ μm (see figure 2(b)), i.e., between the absorption peak for liquid water at $\lambda = 2.94$ μm and the absorption peak of polycrystalline ice at $\lambda = 3.10$ μm. Important desorption yields ($\sim$80% of the maximum) are still observed at wavelengths as short as 2.88 μm. Krasnopoler and George [37] explained this shift by the fact that the ice film melts and remains in the liquid phase during a significant fraction of the laser–ice interaction. This explanation is plausible as the FEL macropulse is composed of several thousands of ps micropulses, for a total duration of 3 μs. One then gets progressive heating of the ice film to liquid in the first micropulses and subsequent desorption from liquid phase for the next ones. The enhancement of the desorption yield for $\lambda < 3.10$ μm is then to be related to a 'dynamic absorption coefficient' attributed to the weakening of the hydrogen-bonding network versus temperature [58, 59].

In contrast to this picture, the OPO desorption pulse duration is 10 ns, i.e., much shorter than the 3 μs duration of the FEL macropulse, which allows a much faster energy deposition, resulting in an explosive phase transition, as presented in section 5.

In addition to these works on pure H_2O samples, a number of studies in the IR-MALDI field investigated the resonant character of the laser desorption process promoted by the O–H stretching. The results of these various studies are very different and surprising at the first sight. In an FEL study on aliphatic and aromatic compounds (succinic, nicotinic, and fumaric acids), Cramer *et al* [17] compared the IR absorption spectra of these compounds with the wavelength dependence of the threshold-fluence (defined as the lowest laser fluence which gave more than 10% of the spectra with analyte signal-to-noise ratio greater than 3:1). The results presented in figures 2–4 of [17] show absolutely no match between the absorbance and threshold-fluence curves. Instead, a curious monotonical increase of the latter is observed over the whole wavelength range investigated (2.8–3.8 μm). These results were contradicted by a newer OPO study [25] which found a low threshold-fluence plateau for succinic and nicotinic acids, leading to somehow better resemblance with the absorption spectrum. This study addressed a high number of MALDI matrices from different chemical classes. A good correlation between O–H absorption and threshold-fluence was found for glycerol and triethanolamine (see figure 5 of [25]), although a $\sim$130 nm blue-shift of the threshold-fluence curve with respect to the absorption one was observed. This result was confirmed in the review paper of Dreisewerd *et al* [28]. Also, Caldwell and Murray [22] had presented a wavelength dependence of the MALDI mass spectra in the 2.76–3.1 μm when using a water/glycerol matrix, but no comparison of the desorption yield or threshold-fluence with the absorption spectrum was available.

Some other studies claimed no effect of the wavelength on the threshold-fluence for succinic and caffeic acids in the 2.9–3.5 μm range [18] or for succinic acid in a shorter 2.88–2.96 μm range [19], although no quantitative comparison with the spectra was presented. The direct comparison presented in [23] shows bad or poor correlation for succinic and caffeic acids. Finally, even a result in complete contradiction with what could be expected in a normal absorbance–fluence picture was obtained by Hess *et al* [21] in an FEL study on succinic acid: the desorption threshold was higher for higher absorbance in the 3 μm region (figure 3 of [21])!

All these contradictory results reflect the necessity of a better investigation of the fundamental processes that could affect the resonant character of the desorption. We note however that a conceptual problem could affect the method used in some MALDI studies, i.e., the comparison between the optical absorption spectra and the inverse of threshold fluences

instead of the desorption yields. For example, Caldwell *et al* [18] claimed no dependence of the threshold fluence on the laser wavelength, while figure 2 of their work shows a clear evolution of the desorption yield, with a marked optimum at 3.0 μm.

3.1.2. Fluence dependence and desorption depth. In addition to the wavelength dependence presented above, the evolution of the desorption yield with the fluence or the thickness of the layer desorbed at each laser shot are important parameters for a complete characterization of the desorption process. In order to determine the desorption depth per laser shot, we implemented an interferometric method to precisely measure the thickness of the ice film grown from vapour phase. Figure 3(a) presents interference fringes recorded for the growth of a 6.8 μm thick ice film; each fringe represents a thickness change of 0.34 μm. The ice film was then completely desorbed by 25 laser shots, as one can see in figure 3(b), which shows the apparition of the substrate (copper) signal in the mass spectrum (see also figure 3(c) for a picture of various desorption spots on the same sample). These numbers lead to a desorption depth per laser shot of $\sim$0.27 μm. It must be emphasized that this value is very close to the penetration depth $z = 1/\alpha = 0.31$ μm obtained when considering the Beer–Lambert law and the absorption coefficient α of ice at $\lambda = 3.1$ μm [60]. Although no precise numbers were derived in the FEL study of Krasnopoler and George [37], significant H_2O signals were recorded for 20 laser shots at 1 mJ/pulse for a 5 μm thick ice film. This would lead to a desorption depth of 0.25 μm/pulse, which is of the same order of magnitude with our OPO results. In a subsequent Er:YAG study [3], Livingston *et al* reported a 0.5 μm/pulse desorption depth for 0.65 mJ/pulse energy at 2.94 μm (note however that at this wavelength the penetration depth is $z = 0.99$ μm [60]).

Figure 4 displays single-shot resonant desorption yields as a function of the idler pulse energy [38]. A desorption threshold of $\sim$0.5 mJ/pulse and a linear evolution of the desorption yield up to 3 mJ/pulse are observed. These results offer then an easy way to normalize signals obtained at different OPO wavelengths with different desorption energies and also to account for the idler shot-to-shot instabilities ($\pm$10%), due to the Nd:YAG pump laser instability.

A linear dependence with a threshold close to 0.5 mJ was also obtained in the FEL study of Krasnopoler and George [37] for an ice film thickness of 5 μm and desorption wavelengths of 2.94 and 3.09 μm. For a 1 μm sample the evolution is less linear for 3.09 μm and not linear at all for 2.94 μm (at this wavelength the film thickness is comparable with the penetration depth, see above). In the Er:YAG study at 2.94 μm [3] a linear dependence was also observed in the 0.5–2.5 mJ/pulse range for a 10 μm thick ice sample at $T = 140$ K. The linear dependence observed in these two works suggests a single-photon mechanism for the IR laser resonant desorption mediated by the O–H stretching mode.

3.2. C–H stretching

In order to evidence the resonant character of the IR laser desorption *via* the C–H stretching mode, pure PAH samples were irradiated by OPO pulses of 1 mJ energy at different wavelengths, in the spectral range between 2.9 and 3.4 μm. PAH molecules have the advantage of being formed only from C and H atoms, thus avoiding the presence of O–H or N–H stretching modes in the vicinity of the investigated C–H one. This is of particular importance for MALDI studies, as it will be discussed below.

Three PAHs were considered for this study, namely naphthalene ($m = 128$ amu), acenaphtene ($m = 154$ amu), and phenanthrene ($m = 178$ amu) [41]. The samples (2 mm thick tablets) were obtained by pressing 300 mg of pure (>98%) ground PAH (Sigma-Aldrich) in a hydraulic press; they were mounted on the temperature-regulated cold finger and cooled down to –170 °C to prevent PAH sublimation under vacuum.

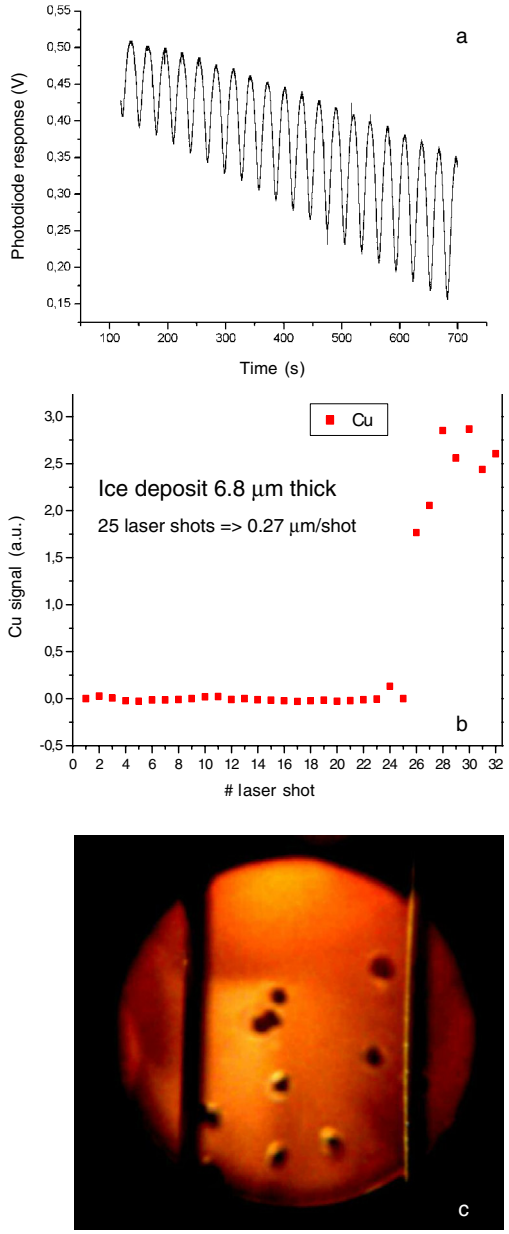

Figure 3. (a) Interference fringes recorded during the growth of an ice sample. Each fringe corresponds to 0.34 μm thickness. (b) Measurement of per-shot desorption rate for ice LRD: 25 laser shots are needed to desorb a 6.8 μm thick ice film, leading to a 0.27 μm/shot desorption rate. (c) Laser resonant desorption traces on an ice film sample.

An excellent agreement between the desorption yield and the C–H absorption spectrum has again been obtained for all the three molecules tested. This strengthens the idea of the resonant character of the laser desorption process *via* C–H stretching energy coupling. As an

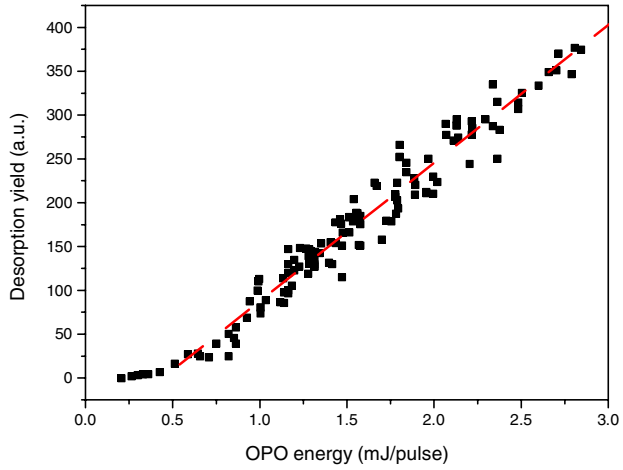

Figure 4. Single-shot desorption yields versus OPO idler pulse energies. The experimental points represent the sum of the M = 1, 16, 17, 18 and 19 amu signals. Reproduced with permission from [38].

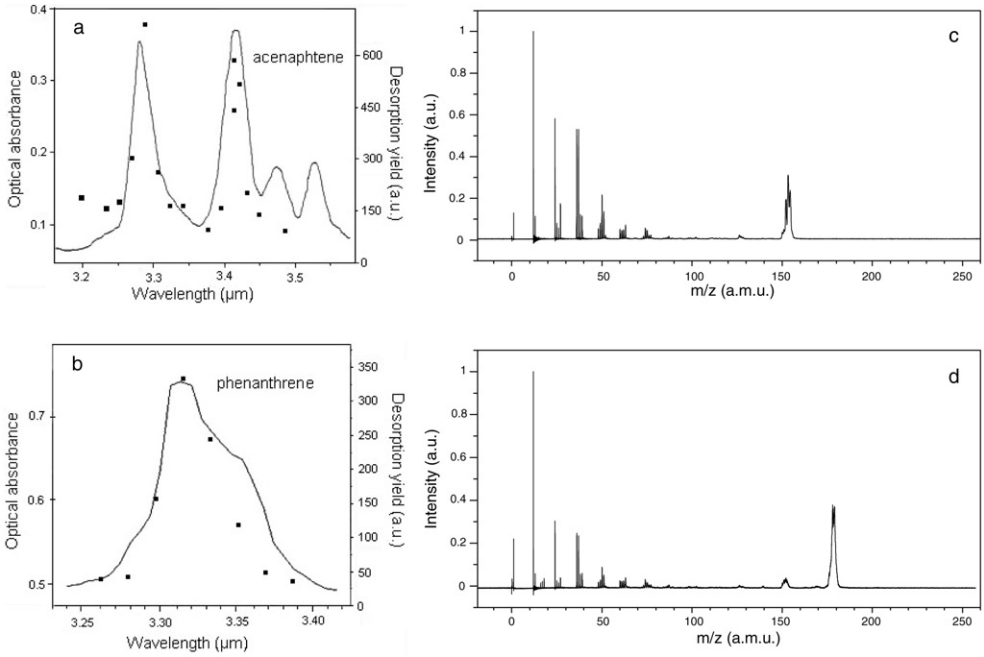

Figure 5. Comparison of desorption yields and optical absorption spectra in the C–H stretching mode region for (a) acenaphtene and (b) phenanthrene. Typical mass spectra obtained by OPO resonant desorption of (c) acenaphtene and (d) phenanthrene. Desorption wavelength: 3.3 μm, desorption energy: 2 mJ/pulse, ionization wavelength: 266 nm, ionization energy: ∼30 mJ/pulse, desorption–ionization delay: 30 μs.

example, figures 5(a) and (b) display the experimental laser desorption yields superimposed on the ∼3.3 μm optical absorption spectra of acenaphtene and phenanthrene, respectively

(condensed phase/solution, data of [61]). In addition, figures 5(c) and (d) display typical mass spectra obtained by laser resonant desorption of acenaphtene and phenanthrene samples (note that all the mass spectra have been normalized, therefore one should not use a direct comparison between the intensities of different PAH signals to evaluate the relative efficiency of the desorption/ionization processes). The effective C–H laser resonant desorption observed for the three PAH molecules, with good signal-to-noise ratio mass spectra, is somehow affected by extensive fragmentation. At a first glance, one can notice a clear segregation between high (over ∼100 amu) and low mass peaks. The high mass peaks are associated to the desorbed PAH and possibly some larger fragments conserving the aromatic ring structure, while the low mass peaks are series of hydrocarbon radicals C_xH_y produced by extensive fragmentation due to the desorption and/or ionization processes or to collisions in the expansion plume. On the other hand, no clustering or in-plume molecular associations have been evidenced: the highest mass signal always corresponds to the molecular weight of the PAH being desorbed. Some indications show the role of the ionization in the fragmentation: in particular, we have observed the presence of all the fragments in mass spectra obtained by sublimation of the solid phase, i.e., without laser desorption. Note also a pronounced broadening of the mass peak profiles at high masses. This broadening is not due to a mass spectrometer fault and its cause is still to be determined. Possible explanations would be the different energetic and thermodynamic properties of PAHs (high mass peaks) with respect to chain hydrocarbon radicals (low mass peaks), but further investigations are necessary to clarify this problem [50].

To our knowledge, only one study addressed the laser resonant desorption character via the C–H stretching on a pure sample: Tro *et al* [39] used an FEL to investigate butane deposited on Al_2O_3 $(11\bar{2}0)$ at 90 K. The resonant desorption spectrum did not reproduce the infrared absorption spectrum of solid butane, as the asymmetric C–H stretches generated a greater desorption yield than expected, compared to symmetric C–H stretches. This discrepancy was attributed to the orientation of butane molecules in an ordered adlayer (coverages used were $\theta = 1$–7 ML) on Al_2O_3 $(11\bar{2}0)$. The orientation in this ordered adlayer could also be determined, when taking into account the polarization of the IR FEL beam. This result illustrates the potential of the laser resonant desorption as a surface sensitive probe. However, a study on thicker butane films would be interesting in order to see the evolution of the symmetric/asymmetric desorption yield with the thickness and the progressive passage to the bulk.

Some of the MALDI works enumerated in the previous section have also addressed the C–H stretching mode. Sheffer and Murray [23] obtained poor correlation between desorption threshold and optical absorption for caffeic acid, and somewhat better for succinic acid; in contrast, good correlation has been obtained for 4-nitroaniline. The difficulties reported by Sheffer and Murray in obtaining mass spectra for caffeic acid at wavelengths higher than 3.05 μm were contested several years later by Menzel *et al* [25], who extended the useful desorption range up to 3.4 μm. These authors also announced a good performance for succinic acid as a MALDI matrix in the 3.3–3.4 μm range, with lower threshold fluences than in the prior studies by Cramer *et al* [17] and Sheffer and Murray [23]. Finally, Dreisewerd *et al* [28] concluded in their review paper that for the C–H stretch vibration mode around 3.4 μm, the spectral courses of the threshold fluences were found to track essentially those of the IR absorption for all matrices.

These results and interpretations are rather contrasted, although less than those for the O–H stretch. Part of the difficulty is represented by the spectral congestion and the relative low band strength of the C–H mode (compared to the stronger close-lying O–H absorption). As said above, this illustrates the necessity of fundamental studies on molecules containing exclusively C and H atoms (e.g., PAHs or butane) in order to investigate the C–H stretching mode alone.

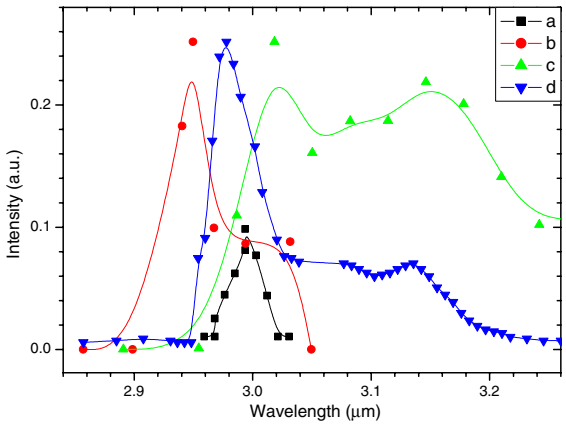

Figure 6. Comparison of NH_3 desorption yields (DYs) and optical absorption spectra in the N–H stretching mode region: (a) DY for a 1 ML NH_3 adsorbed on Cu(100) at 90 K (data from [43]). (b) DY for a 2 ML NH_3 adsorbed on Ag film at 10 K (data from [43]). (c) DY for a thick ($\sim$100 μm) NH_3 film deposited at 90 K (present work). (d) Optical absorption spectrum of a 0.72 μm thick NH_3 film deposited at 10 K (data from [62]).

3.3. N–H stretching

The resonant photostimulated desorption via the N–H stretching in the 3 μm region was the first non-CO_2 laser work in this field. In the early eighties, Chuang and co-workers used a tunable difference-frequency generation source to investigate the laser desorption of NH_3 thin layers deposited on Cu or Ag surfaces [42, 43]. They evidenced the resonant character of the desorption yield (see figure 6, traces (a) and (b)). Moreover, the resonance profile has been found to depend (in position and shape) on the coverage and substrate nature (see figures 4 and 9 of [43]). The presence of two distinct mechanisms (single-photon and thermal) involved in promoting desorption has been claimed.

With the development of the MALDI technique in the IR, several studies have addressed the wavelength behaviour of the desorption performance of different matrices involving the N–H stretching mode. Sheffer and Murray [23] found a qualitatively good correlation between the inverse of the threshold fluence and the IR absorption spectrum of 4-nitroaniline, although the threshold fluence at 2.9 μm was lower than expected. Sadeghi *et al* [19] performed a wavelength scan over the absorption bands of urea around 2.95 μm, but no influence of the IR spectrum modulations was detected on the MALDI mass spectra. Menzel *et al* [25] obtained the same kind of behaviour for thiourea. For amino acid tryptophane, the same authors found a better correlation between the absorption spectrum and the MALDI threshold wavelength dependence, although the MALDI feature was somewhat broadened (see figure 4 of [25]).

We performed preliminary studies on the resonant character of the N–H promoted desorption using thick ($\sim$100 μm) films of NH_3 deposited from the gas phase on Cu substrate at 90 K. The wavelength dependence of the desorption yield is displayed in figure 6 (trace (c)). A pronounced broadening with respect to the early studies of Chuang and coworkers [42, 43] is observed. Our results seem rather to confirm the trend observed in the more recent MALDI investigations. However, in contrast with our findings on the O–H and C–H stimulated desorption, the N–H desorption yield does not replicate the IR absorption curve of NH_3 (displayed for comparison in figure 6 (trace (d), data from [62])). The reason for this deviation is not clear yet and supplementary experiments are underway in order to understand it.

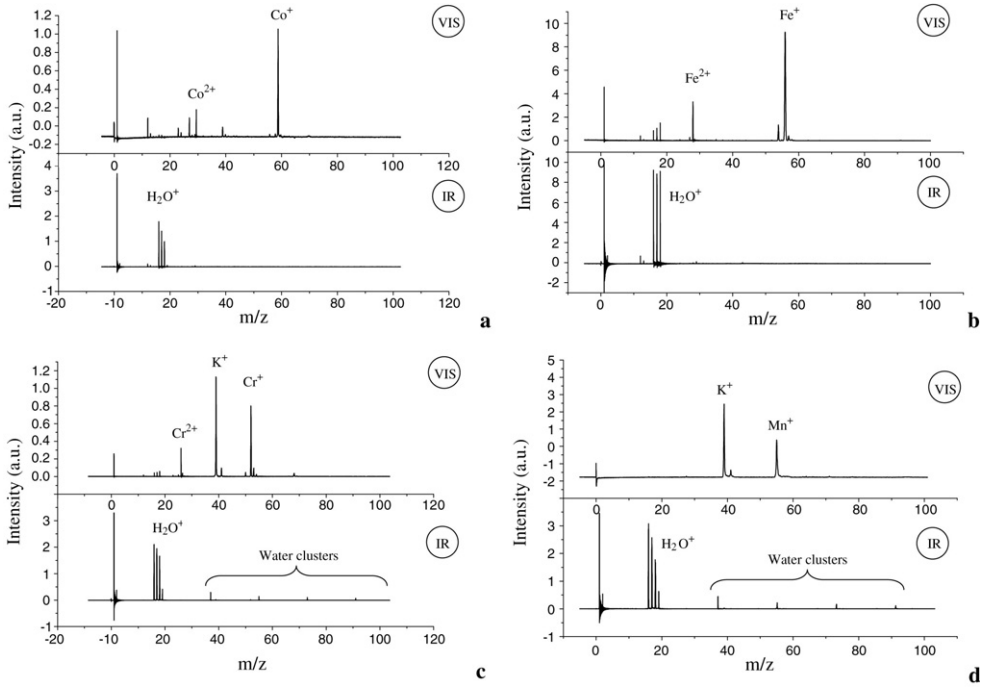

Figure 7. Laser desorption mass spectra of ice/metal salt binary systems at two different desorption wavelength, $\lambda = 532$ nm (VIS) and $\lambda = 3.1$ μm (IR): (a) $CoCl_2$ 0.5 M, $E_{VIS} = 50$ mJ/pulse, $E_{IR} = 2$ mJ/pulse; (b) $FeCl_3$ 0.5 M, $E_{VIS} = 45$ mJ/pulse, $E_{IR} = 2$ mJ/pulse; (c) $K_2Cr_2O_7$ 0.3 M, $E_{VIS} = 6.5$ mJ/pulse, $E_{IR} = 2$ mJ/pulse; (d) $KMnO_4$ 2×10^{-3} M, $E_{VIS} = 7$ mJ/pulse, $E_{IR} = 2$ mJ/pulse. Reproduced with permission from [47].

4. Laser desorption of binary mixtures

4.1. Wavelength-selective desorption

The resonant character evidenced above can be employed to attempt the selective desorption of one component from a complex mixture. This was done in two separate studies: the first one dealt with visible/IR selective desorption of metal salt/ice binary mixtures [47], and the second one investigated the IR/IR desorption of a PAH/ice mixture *via* the C–H and O–H stretching modes [40].

In the first study, a series of frozen metal salt ($K/Na(MnO_4)$, $K_2Cr_2O_7$, $FeCl_3$, $CoCl_2$) aqueous solutions with different concentrations (in the range 3×10^{-4} M–0.2 M) were used as test samples. Each sample was successively irradiated with visible (532 nm) and IR (3.1 μm) beams, and the desorption products of each experiment were multi-photon ionized (266 nm) and detected by time-of-flight mass spectrometry in identical experimental conditions. All the metal salts listed above present a significant absorption coefficient at the visible wavelength employed (532 nm), as one can see from the spectrophotometric measurements summarized in figure 1 of [47].

Figure 7 displays the mass spectra recorded following VIS/IR laser desorption for four of these solutions (the results for sodium permanganate are similar with those for potassium permanganate). The VIS/IR mass spectra were acquired by irradiating different fresh areas of the sample surface. The striking difference between the two irradiation regimes is noticeable

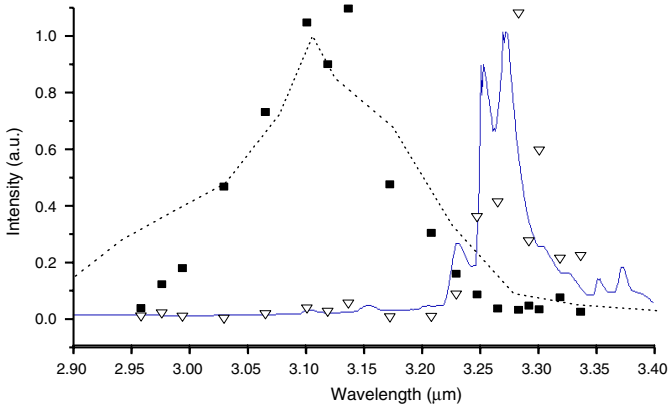

Figure 8. Experimental desorption yields for water (■) and naphthalene (▼) in the 2.9–3.4 μm wavelength range compared to the optical absorption spectra of ice (dotted line, 100 K, data from [57]) and naphthalene (solid line, 15 K, data from [63]). The experimental desorption yield values for naphthalene have been magnified by a factor of four (see text).

at first glance. Under IR exposure, the only signals in the mass spectra are those corresponding to the water molecule ($m/z = 18$), its fragments OH $m/z = 17$ and O $m/z = 16$ (extensive fragmentation is present due to the choice we made to use high ionization pulse energies in order to get maximum sensitivity), and its clusters $H_3O^+(H_2O)_n$. In contrast, when the samples were exposed to visible radiation, almost no water signal was evidenced, and high metal atom signals appeared.

To our knowledge, this is the first time that such a behaviour has been evidenced in a direct manner, and its explanation seems quite puzzling at a first approach. The principle of the simultaneous co-desorption of the solute and the matrix molecules represents the base-stone itself of a technique like matrix assisted laser desorption and ionization (MALDI). The concentrations used here are at least of the same order or even higher than those usually employed in MALDI ($\sim 10^{-4}$ M). For instance, a 2×10^{-3} M $KMnO_4$ solution (used in this work) implies one K or Mn atom for about 3×10^4 water molecules. A tentative description of the desorption mechanisms involved will be given in the next sections, along with possible analytical and technological applications.

The wavelength-selective desorption phenomenon has been confirmed in a recent IR/IR study on ice/PAH (naphthalene) mixtures [40]. The cryogenic samples ($H_2O/C_{10}H_8$ ratios of $\sim$100) were irradiated by IR OPO pulses of 1 mJ energy at 18 different wavelengths, in the spectral range between 2.9 and 3.4 μm. For each wavelength, 100 mass spectra were averaged and the amplitude of $m/z = 18$ amu (water) and $m/z = 128$ amu (naphthalene) peaks was measured.

The desorption yields measured for different wavelengths in the spectral range investigated are displayed in figure 8, along with IR absorption spectra of ice (100 K, data from [57]) and naphthalene (15 K, data from [63]). In order to make the experimental data easily comparable, the values recorded for naphthalene have been magnified by a factor of 4 (note that the strength of the O–H band is largely superior to that of the C–H band [63]). Figure 8 clearly evidences the wavelength-selective character of the laser desorption process (this can also be noticed from the mass spectra recorded at $\lambda = 3.13$ and 3.28 μm; see figure 2 of [40]). Highly preferential desorption of water molecules and its fragments is observed when in resonance with the O–H mode (3.13 μm), while almost exclusive desorption of naphthalene and carbon-based fragments is recorded in the C–H mode resonance (3.28 μm).

It must be emphasized that the selective character of the laser desorption of binary mixtures was achieved in specific conditions of laser fluence and solution concentration. Varying these parameters can lead to decrease in selectivity, as presented below.

4.2. Loss of selectivity. Cluster generation

4.2.1. The effect of concentration and/or desorption laser fluence increase. To get better insight on the problem exposed above, laser desorption at different laser pulse energies and solution concentrations was performed [47]. Increasing one or both of these parameters led to the same consequence: the loss of the selective character of the desorption process. This is illustrated by the mass spectra displayed in figure 3 of [47] for (a) a concentrated (0.2 M) $KMnO_4$ solution, exposed to 7 mJ/pulse 532 nm irradiation and (b) a relatively low concentration (2×10^{-3} M, the same as in figure 7(d) of the present paper) $KMnO_4$ solution, exposed to 40 mJ/pulse 532 nm irradiation. The appearance of a water signal and extensive $K(H_2O)_n$ clustering is observed in both cases. Also, an intense unresolved signal occurs before the laser ionization pulse, i.e., it corresponds to direct ionization simultaneous with the desorption. The extensive clustering observed confirms previous results obtained in our group on $Na/KMnO_4$ doped ices [49] or other different ice-based mixtures [45, 46]; this issue will be addressed later.

Unfortunately we have not yet been able to perform the same study for the IR desorption, as our OPO output has been limited at 2.5 mJ/pulse. However, increasing the laser pulse energy to this value at $\lambda = 3.1$ μm led to more PAH desorbed [40], confirming the trend suggested by the visible desorption. On the other hand, the concentrations used for the IR/IR study (typically 1 PAH molecule for 100 water molecules) were about two orders of magnitude higher than those employed in the inorganic salt/ice experiments [47].

The subsequent idea is that the wavelength-selective regime is closely dependent not only on the laser fluence, but also on the nature of the dopant (contaminant) and its specific relationship to the matrix (substrate). Moreover, along with the laser fluence, the optical absorption coefficient of the sample plays a crucial role. When both absorption coefficient and laser fluence are high this can lead to the sample destruction by ablation and formation of craters, as one can see in figure 4 of [47]. The two regimes (desorption versus ablation) have been recognized by Yingling *et al* [64] in a combined experimental/theoretical study on UV (248 nm) laser desorption of binary mixtures. Dimethylether (volatile) and decane (non-volatile) have been used as solutes in a toluene matrix (only the matrix absorbed the 248 nm radiation). Preferential desorption of the volatile compound has been evidenced in the low-fluence regime, while co-desorption occurred once the ablation threshold has been passed, confirming previous experimental [65, 66] and theoretical [67–69] studies. However, these results differ from ours in that the preferential ejection is studied in terms of volatility, but not by varying the laser wavelength to achieve resonant desorption of one or the other of the binary mixture components. In our approach, the final hint is that one can control the desorption products by choosing the adequate wavelength and a laser fluence in a range defined by the selective desorption and the ablation (co-desorption) thresholds. This is of practical importance in technological applications, such as pulsed laser cleaning (see section 6.3).

4.2.2. Hydrated cluster generation. In the frame of our laser desorption work on ice-based samples, we observed the formation of long series of hydrated clusters. Although this process occurs in the co-desorption regime, the brief survey proposed below can be useful to illustrate the capabilities of the IR OPO desorption technique, and also as a preamble for the understanding of some aspects of the desorption mechanisms presented in section 5. From a

fundamental point of view, the study of increasing size clusters offers the opportunity to get insight on the transition from the isolated molecule to the emergent condensed phase. In this context, the hydrated clusters are of particular importance: indeed, if water is one of the most familiar elements, its condensed phase presents peculiar macroscopic properties which are not yet well understood in terms of microscopic properties of the individual molecules composing it and/or in terms of interactions between these molecules. On the other hand, hydrated clusters exist in our environment, for example in the atmosphere as precursors for the formation of droplets in the clouds.

With these motivations, we present below the main results obtained in our group on the different systems considered. All these experiments involved samples obtained by freezing of aqueous solutions of different concentrations (see [40, 45–49] for more precise experimental details).

Alkali atoms. In a first study [49] on alkali salts ($Na/K(MnO)_4$) doped ices, we evidenced the formation of long series of $Na/K(H_2O)_n$ clusters, with n up to ∼30 (see figure 9(a)). The particularity of this study (with respect to the following ones) was the use of a visible (532 nm) laser as desorption source. The two alkali salts were specifically chosen for their important optical absorption coefficient at the desorption wavelength employed. In this case the solute (not the matrix) absorbed the laser radiation. This study included a size and velocity distribution analysis. Also, a temperature investigation showed the independence of the generated clusters on the cryogenic sample temperature.

Formaldehyde. Long series of formaldehyde-based hydrated clusters (with as many as 40 water molecules) were obtained by IR OPO resonant desorption of H_2CO–H_2O cryogenic samples [45, 46]. The cluster series observed were assigned to protonated and deprotonated formaldehyde hydrated complexes $H_3CO^+(H_2O)_n$ and $HCO^+(H_2O)_n$, as well as to mixed $H_3CO^+(H_2CO)_p(H_2O)_n$ and $HCO^+(H_2CO)_p(H_2O)_n$ forms. However, only the $p = 1$ series was definitely assigned for the protonated form, while the $p = 1$ and 2 series were identified for the deprotonated form (see [46] for details). These studies were conducted in parallel with Raman investigations dedicated to structural characterization of droplet congelation [70, 71] The cluster formation mechanism could be correlated with the presence of oligomers in the original liquid solution [70]; their presence in solid phase has been recently evidenced by micro-Raman spectrometry [71].

Methanol and ethanol. Several studies [72–77] reported the generation of methanol/ethanol (hydrated) clusters by SIMS/FAB techniques applied to frozen concentrated solutions of these compounds (water present as impurity). The study we carried out on diluted solutions [45] was the first (to the best of our knowledge) to employ laser desorption for the generation of such complexes. The observed peaks were assigned to cluster series of the form $[MH]^+(M)_p(H_2O)_n$, with M = Me = CH_3OH for methanol and M = Et = CH_3CH_2OH for ethanol. The recorded ranges for p and n were: $0 \leqslant p \leqslant 6$ and $0 \leqslant n \leqslant 12$ for Me, and $0 \leqslant p \leqslant 7$ and $0 \leqslant n \leqslant 7$ for Et. The hydration of methanol and ethanol is less extended than in the case of formaldehyde; instead a larger degree of 'self-clusterization' is obtained for both alcohols considered. Moreover, only the protonated form of ethanol and methanol led to formation of complexes, while both protonated and deprotonated forms were 'cluster active' in the formaldehyde experiment. These observations point out the dependence of the clustering process on the class of organic molecules incorporated into the ice sample (at least for aldehydes and alcohols) and are in general agreement with the previous studies [72–77]. Note, however,

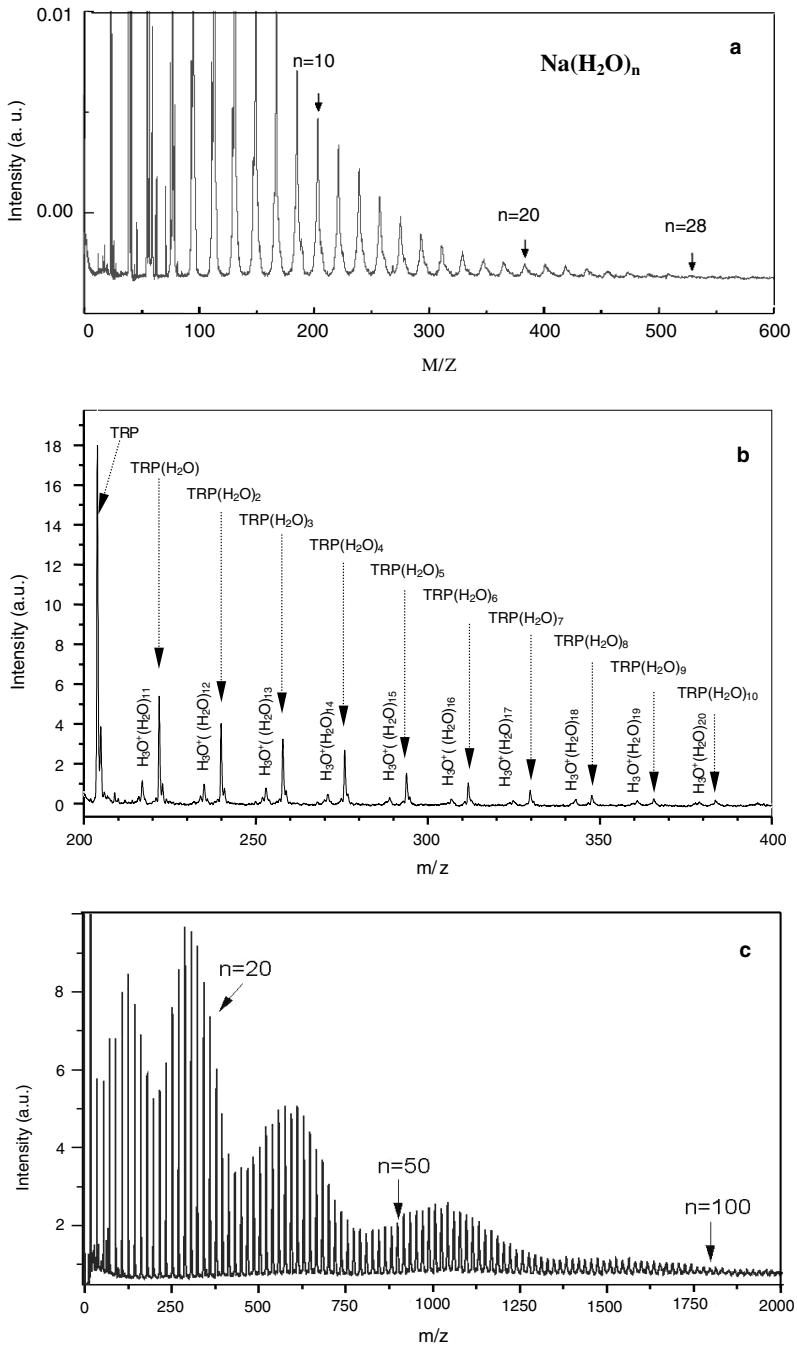

Figure 9. (a) $Na^+(H_2O)_n$ clusters generated by visible (532 nm) laser desorption of a concentrated (0.2 M) $NaMnO_4$ aqueous solution frozen at 150 K. Reproduced with permission from [49]. (b) Hydrated tryptophan clusters generated by IR OPO resonant desorption of a frozen ($T = 90$ K) Trp-H_2O solution (1 wt%). Reproduced with permission from [45]. (c) $H_3O^+(H_2O)_n$ clusters obtained by 3.1 μm laser resonant desorption of a frozen water sample at a temperature of 90 K. Reproduced with permission from [48].

that all the SIMS/FAB experiments revealed a strong dependence of the cluster generation on the sample temperature, as meaningful mass spectra were recorded only in a specific range of several tens of degrees. The authors interpreted this behaviour as indicating that transition to the liquid phase is a necessary step for the mixture considered [72–76]. In our laser desorption study very good quality spectra are obtained at 90 K, where the sample is clearly solid. No notable change was observed with increasing the temperature (in the range 90–190 K), confirming our previous results on inorganic hydrated clusters (see figure 4 of [49]). This represents a significant advantage of the laser desorption technique on the SIMS/FAB methods, as highly hydrated clusters can be generated directly from solid samples at low temperatures, thus avoiding the inherent problems high vapour pressure poses to the use of mass spectrometers.

Tryptophan. As one of the few aromatic amino acids, tryptophan (Trp) plays a crucial role in the UV spectroscopy of peptides and proteins, as illustrated by numerous studies (see, e.g., [78–80]). Several authors proposed laser desorption methods to volatilize this thermally labile molecule (or its peptide), either for use in subsequent spectroscopic studies [81–83] or fundamental laser desorption research [6, 84, 85]. However, to our knowledge, only one study [82] has used this technique to generate tryptophan–water clusters, as an alternative to the classical thermospray or thermal evaporation methods [78–80, 86, 87]. This was done by seeding the laser desorbed material from a solid Trp-containing target into an argon/H_2O supersonic jet. Surprisingly, only one cluster (namely, Trp-$(H_2O)_3$) was obtained in this experiment (see figure 8 of [82]). The authors tentatively explained this behaviour by the zwitterionic character of tryptophan [82]. In contrast with these previous results, our experiments lead to a well-developed, complete series of Trp-$(H_2O)_n$ clusters, extending to ∼20 water molecules associated to one tryptophan molecule. Figure 9(b) shows a portion of the mass spectrum recorded, clearly exhibiting the presence of Trp hydrated complexes.

'Pure' water clusters. The presence of these aggregates is a constant in all our IR OPO desorption studies performed on different samples [38, 45–48]. Figure 9(c) shows a typical cluster mass pattern obtained with our technique from a pure ice sample; one can notice the presence of large $H_3O^+(H_2O)_n$ aggregates ($n > 100$). The generation of water clusters has already been reported in a previous FEL IR-MALDI experiment (at 5.9 μm) for the desorption of biomolecules from ice, but of significantly lower ($n < 20$) size [27]. The abundance of high-mass clusters in our experiment allowed us to perform a thorough investigation on the formation mechanism [48]; this is presented in the next section.

Practical implications and perspectives. The results presented above illustrate the high potential of our IR resonant desorption technique to generate large hydrated clusters of atoms and molecules directly from the ice matrix, thus avoiding the use of complicated crossed molecular beam apparatus. Note that all our works on cluster generation were done on frozen aqueous solutions. We have indeed observed that the use of this type of samples greatly favoured the formation of large clusters, in comparison with the gas-phase deposited samples. For example, a long series ($n > 100$) of $H_3O^+(H_2O)_n$ clusters has been obtained from frozen waters samples [48], while n has been limited to no more than 30 for gas-phase deposits [38]. It seems that the presence of defects and cracks in the frozen samples facilitates the cluster formation. This is in agreement with a model developed by Kosevich and co-workers [76, 88, 89] to describe the mass spectra obtained by fast atom bombardment (FAB) of mixed water–organic compounds at low temperature. Note finally that another interesting

approach for the generation of hydrated clusters with IR laser beams has been proposed by Sobott *et al* [90]. They used the output of a $LiNbO_3$ OPO/OPA in the 3 μm region to generate ionic hydrated clusters (clathrate-like structures) of alkali metal atoms and ammonium from a thin jet of supercooled aqueous solutions in high vacuum (liquid beam ionization/desorption mass spectrometry).

From a practical point of view, the clusters so produced can be subsequently used in spectroscopic studies by UV or IR laser probing (note for example that the spectroscopic investigations conducted up to now on the Trp-$(H_2O)_n$ complexes [82, 86] have been limited to $n \leqslant 2$). Another possibility is opened for structural investigations, by selective trapping of the clusters on catch plates, followed by Raman, x-ray or AFM probing [91].

An important application of the generated clusters is the study of the size distribution, which can offer precious information on their stability and structural properties or on the formation mechanisms. We can observe in figure 9 that the clusters abundance is characterized by successive local maxima and minima. This behaviour has been observed for all the systems presented above; a more detailed treatment can be found in [46, 49]. As a general rule, the size distribution is represented by the sum of several log-normal functions (one for each bell-shaped profile around a local maximum). This is a characteristic of aggregation processes [92]. According to Wang *et al* [93], each log-normal curve corresponds to a distinct structural configuration and the transition to a new curve coincides with a new geometry of the molecular aggregate. Theoretical investigations on water clusters suggested the presence of chain-like structures for the small-size aggregates, which can further develop in cage-like structures for sizes as small as $n = 8$ (see [94] and references therein). The intermediate size aggregates are often modelled by eight-molecule cages. Our results [46] seem to be an argument in this direction. On the other hand, recent experimental results obtained by IR dissociation spectroscopy of water clusters [95, 96] or benzene–water complexes [97] suggest a chain structure up to $n \sim 10$, which develops further in a 2D network for $10 < n < 20$ and completes the 3D cage at $n = 21$, with the aromatic compound [97] expulsed from the cage. Let us note finally that numerous authors (see, e.g., [98, 99]) evidence the presence of 'magic numbers', i.e., aggregates of high stability compared to their neighbours in the series. Our mass spectra do not seem to show the occurrence of these magic numbers for the clusters obtained by IR laser desorption of ice matrices. This must however be confirmed in the future by a finer analysis at the post-ionization fragmentation (metastable decay) level, by taking advantage of the presence of a reflectron on our time-of-flight mass spectrometer.

5. Insights on the desorption mechanism

5.1. Ejecta velocity distribution

The data concerning the velocity distribution of the ejecta (and, more generally, the desorption plume dynamics) are, along with the more classical approach in terms of incident flux [7], of fundamental importance for the understanding of the laser–matrix interactions (see, e.g., the MALDI studies [100–102]). In our experiment, the velocity distribution of the desorption products can be recorded by varying the Δt delay between the desorption and ionization lasers. In this way molecules with different velocities will be ionized.

A common trend has been observed in all the velocity distributions recorded for various ice-based systems (desorption promoted by the O–H stretching). A steep rise of the signal has been recorded at Δt delays of 15–25 μs, followed by a much slower decay, up to several hundred microseconds. If one considers the $\Delta z = 35$ mm distance between the desorption and the ionization points, this turns into velocity values $v = \Delta z/\Delta t$ between

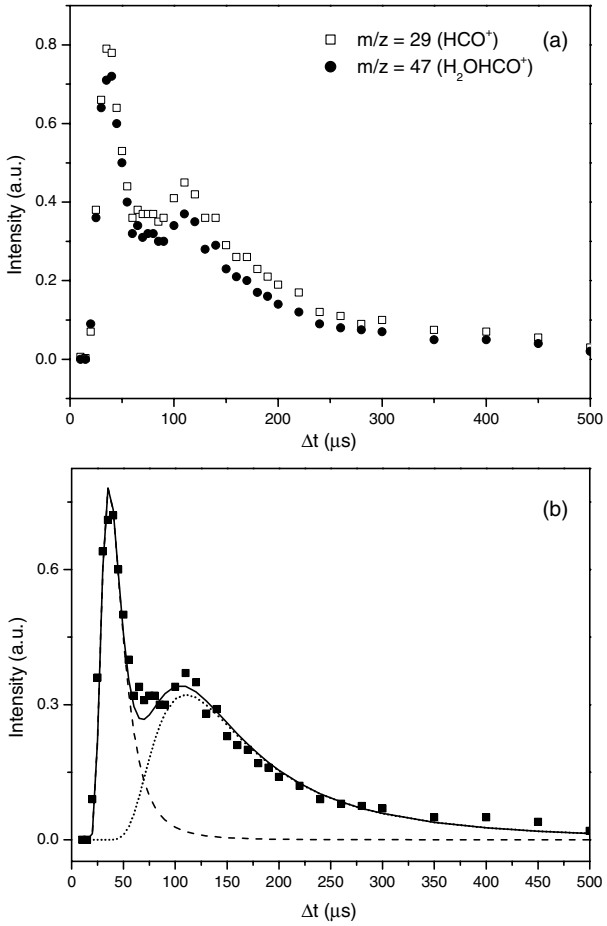

Figure 10. (a) Time of flight distribution for the desorption products HCO^+ (m/z = 29) and H_2O–HCO^+ (m/z = 47) obtained by O–H IR-LRD of a frozen aqueous solution of formaldehyde [46]. (b) Fit of the experimental points by a sum of 'shifted' and 'classical' Maxwell distributions (see text for details). Reproduced with permission from [46].

$\sim$100 and $\sim$2500 m s^{-1}. As an example, figure 10(a) presents the Δt evolution of the signals $m/z = 29(HCO^+)$ and $m/z = 47(HCO^+–H_2O)$ obtained in the study of the formaldehyde–ice system (3.1 μm laser resonant desorption, [46]). One can easily notice the presence of (at least) two components (a 'fast' one and a 'slow' one) in the velocity profile, characterized by the two local maxima. Multiple-component velocity distributions have already been recorded by several authors [103–110]. Different interpretations have been proposed, in terms of thermal/non-thermal mechanisms [103–105], thermal subjacent processes [105, 106], 'hyper-thermal' versus 'near-thermal' desorption [107, 108], or even as a consequence of reaction products formation [109, 110]. A simplified view would be to consider the very fast heating of the solid by the laser energy deposited, leading to the instant 'explosive' vaporization of a sample micro-volume, followed by a slower thermal dissipation in the surrounding volume, leading to a 'normal' vaporization due to the temperature rise.

Another observation to be made when looking to figure 10(a) is the exact temporal coincidence of the two profiles ($m/z = 29$ and $m/z = 47$). This situation (different

masses exhibiting the same velocity distribution) has already been reported in laser desorption (experimental [65, 111, 112] and theoretical [113, 114]) studies on binary systems. This behaviour is explained by the simultaneous ejection of matrix and solute molecules (or aggregates) followed by thermalization due to collisions and represents one of the main characteristics of the Kelly's model presented below. Moreover, in our case, this observation gives a supplementary proof on the common (solid phase) origin of HCO^+ and HCO^+–H_2O, as will be developed later.

5.2. Kelly's model: surface temperature and phase explosion

The fast component of the velocity profile corresponds to an 'explosive vaporization' and can be accounted for by a Maxwell-like distribution superimposed on a stream velocity u_z :

$$f(v_z)\,\alpha v_z^3 \exp\left[-\frac{m}{2kT}(v_z - u_z)^2\right] \tag{1}$$

where $v_z = \Delta z/\Delta t$ is the axial velocity, k the Boltzmann constant, and T the translation temperature of the probed species at the ionization point (note that following the demonstration of Kools *et al* [115] a v_z^3 pre-exponential has been adopted, as it is appropriate for a density-sensitive detector). The slow component of the velocity distribution is associated with a 'normal vaporization' and a classical Maxwell function suffices to describe it (i.e., no stream velocity, $u_z = 0$ in equation (1)).

The explosive vaporization regime has been depicted in a model developed by Kelly and co-workers [116–124]. This model is based on the formation of a Knudsen layer, i.e., a spatial region next to the sample surface in which each desorbed particle will exhibit several collisions leading to the transformation of the initial 'half-space' ($v_z \geqslant 0$) velocity distribution (present at the desorption moment) in a 'full-space' ($-\infty < v_z < \infty$) Maxwellian distribution superimposed on the stream velocity u_z. The Knudsen layer border is defined by a Mach number $M = 1$, i.e., the stream velocity equals the sound speed a:

$$u_z^{\mathrm{KL}} = a = \sqrt{\frac{\gamma k T_{\mathrm{KL}}}{m}} \tag{2}$$

where γ is the adiabatic coefficient C_p/C_v (=4/3 for H_2O molecules) and T_{KL} the temperature at the Knudsen layer limit.

Beyond this limit a supersonic expansion occurs, characterized by the Mach number:

$$M = \frac{u_z}{a} = u_z\sqrt{\frac{m}{\gamma kT}}. \tag{3}$$

Equation (1) may then be rewritten in the equivalent form:

$$f(v_z) = v_z^3 \exp\left[-\frac{\gamma}{2}M^2\left(\frac{v_z}{u_z} - 1\right)^2\right]. \tag{4}$$

Measuring M and u_z (or T and u_z) at the ionization point allows one to derive the T_{KL} temperature at the Knudsen layer limit by means of the well-known relationship [125]:

$$T_{\mathrm{KL}} = T\left[1 + 1/2(\gamma - 1)M^2\right]. \tag{5}$$

Finally, the surface temperature at the desorption moment can be deduced from an equation which accounts for the processes taking place in the Knudsen layer [118]:

$$(T_{\mathrm{KL}}/T_{\mathrm{S}})^{1/2} = -\frac{(\pi\gamma/2)^{1/2}}{2\,(j+4)} + \left[1 + \frac{\pi\gamma/2}{4\,(j+4)^2}\right]^{1/2} \tag{6}$$

where j is the number of degrees of freedom of the considered species. For water molecules one gets $T_{KL} = 0.81T_S$.

The dashed line in figure 10(b) represents the fast component (equation (4) with $M = 2$ and $u_z = 700$ m s^{-1}), while the dotted line accounts for the slow component (equation (1) with T = 190 K and $u_z = 0$ m s^{-1}); the solid line is the sum of the components. One can note the excellent agreement between the experimental data and the theoretical curve based on Kelly's model.

The values derived for the fast component are typical for all our works on pure or doped ice samples [38, 45, 46, 48, 49]. In this series of studies, Mach numbers between 1.7 and 2 and stream velocities in the range 700–1100 m s^{-1} have been obtained. Using the model outlined above, surface temperatures between 504 and 650 K have been found. These values are close to the critical temperature of water ($T_C = 647$ K) and represent a strong argument for the phase explosion mechanism. It has indeed been proven [122, 123] that beyond a temperature of about 0.85 T_C an extensive homogeneous nucleation occurs, leading to a fast expulsion of a micro-volume of the solid sample into the gas phase. We note however that a phase explosion process has been observed recently by shadowgraphy [126] in a water jet vibrationally excited at 1.9 μm for significantly lower (far from spinodal) temperatures (measured by Raman spectroscopy). Moreover, no homogeneous nucleation has been observed in the liquid volume (but this can be due to optical limitations).

The slow ($T = 190$ K) component of the velocity distribution corresponds to a 'normal vaporization' regime [123]. Velocity distributions with low-temperature (100 K) components have already been reported experimentally [105]. We must however stress that this process is more complex than the phase explosion: while there is a unique threshold temperature (close to the critical temperature) for the latter, in the case of the normal vaporization the surface temperature is not defined to the same extent, i.e., this process can take place in a wider temperature range. For this reason, it is somehow artificial to derive vaporization temperatures from these types of data [124].

The presence of two different regimes (phase explosion and normal vaporization) in our laser desorption experiments on ice-based systems is now well established. On the other hand, the similar values (in terms of T_S, M, u_z) found in all our studies illustrate the idea (recently proven in MALDI experiments [100–102]) that the velocity distribution is a characteristic of the matrix employed, with little or no dependence on the solute or on the laser fluence (given this latter is superior to a specific threshold, i.e., in the co-desorption regime).

5.3. Cluster formation

In order to get a more precise image of the cluster formation mechanism, we studied the evolution of the velocity distribution with the cluster size [48]. This has been done on the pure water $H_3O^+(H_2O)_n$ cluster series, which is well developed and exhibits intense reproducible signals for high masses. Figure 11 presents the velocity distributions for three light $H_3O^+(H_2O)_n$ clusters (with $n = 1$, 3 and 6) and two heavier ones, $H_3O^+(H_2O)_{35}$ and $H_3O^+(H_2O)_{40}$, obtained in conditions identical to those previously presented. While the distributions of the first clusters is similar to those found in previous studies (presence of two main components, comparable u_z stream velocity), the heavier clusters' velocity distribution is different in that no fast component is observed. This finding is in agreement with recent molecular dynamics simulations developed by Zhigilei [127]. This theoretical work evokes indeed a clear segregation between light and heavy clusters. The former would be ejected from the sample surface with high velocity (due to the phase explosion mechanism, as suggested by our work), while the latter would originate from a small volume underneath the surface with a

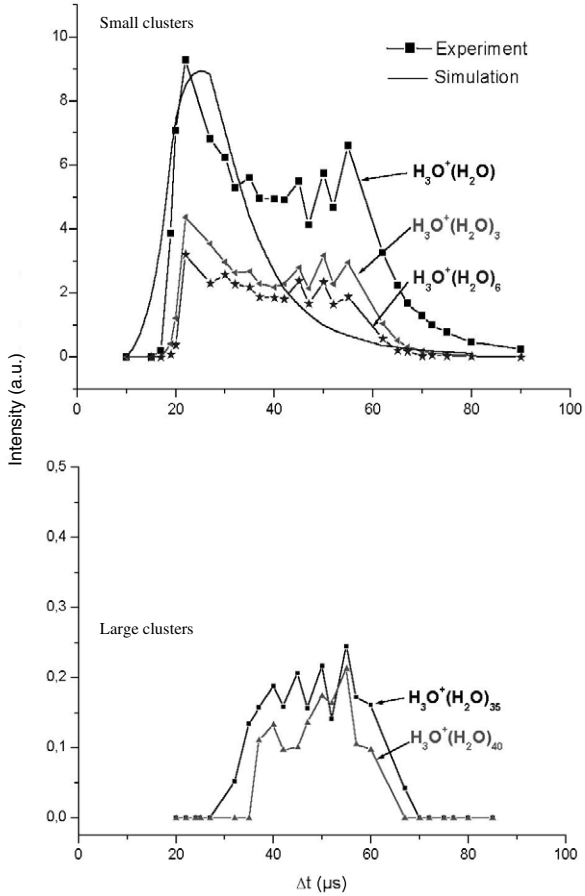

Figure 11. Velocity distribution of three small (top) and two large (bottom) water clusters. Reproduced with permission from [48].

lower velocity (resulting only from the normal vaporization mechanism), the slower aggregates ($\Delta t > 70\ \mu$s in our case) having an important probability of dissociation before their detection.

This last hypothesis is confirmed by a new experiment in which we followed the evolution of several clusters with the Δz distance between the desorption and ionization points (see figure 4 of [48]). It is observed clearly that the heavier clusters contribution diminishes when they spend more time in the plume, this revealing unambiguously a fragmentation process of this clusters in monomers and smaller size aggregates. This is a supplementary contribution to the slow decay (up to $\Delta t > 200\ \mu$s) of the velocity distribution of water monomers observed in similar experiments.

5.4. Discussion

5.4.1. O–H versus C–H desorption. The scenario presented above has been observed in all our O–H mediated IR desorption studies [38, 45–48]. Surprisingly, the picture looks quite different in the case of C–H mediated desorption [41]: non-negligible signals are observed at

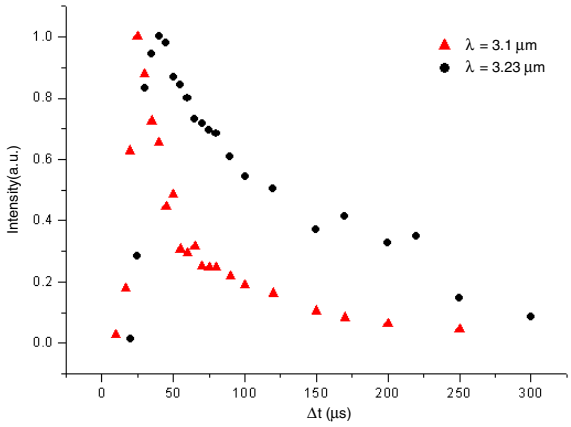

Figure 12. Velocity distribution of water molecules desorbed at two different wavelengths: (▲) 3.1 μm and (●) 3.23 μm.

high Δt delays (more than 50 ms; see figure 3 of [41]). This is orders of magnitude higher than in the case of the O–H studies, where the desorption plume has been limited to several hundreds of μs (working in the same experimental conditions, i.e., 10 ns desorption pulses and $\Delta z = 35$ mm desorption–ionization distance).

Several factors could contribute to this unexpected long-term ejection: the different thermal properties of the PAH samples (e.g., PAHs are known as very good thermal insulators) or the optical absorption strength of the C–H band, which is about two orders of magnitude lower than that of the O–H one [63]. From the thermal point of view, the laser energy transfer to the sample through the C–H mode is fast (∼ps), so thermal equilibration of the system is probably achieved on the timescale of the laser pulse and the main difference should therefore appear at the heat diffusion and evaporation level. The other working hypothesis is situated at the optical level: indeed, the low optical absorption coefficient of the C–H mode turns into higher penetration depth values. The volume affected is then larger, but the energy available per volume unit is lower. This would lead to less heating of the sample, i.e., the temperature would not increase enough to initiate the phase explosion process.

In order to investigate the optical hypothesis, some work has been done in the O–H absorption profile at different wavelengths (i.e., different absorption coefficients). Figure 12 presents the velocity distributions obtained at 3.1 μm (maximum of the absorption profile) and 3.23 μm (wing of the absorption profile). A clear rise in the slow component contribution is observed for the lower absorption coefficient, confirming the supposed trend. These investigations are now completed by work in the C–H profile, and will be published separately.

Finally, another cause for the long-tail distribution observed could be the in-plume processes (note however that no clustering was observed in the C–H study [41], in contrast to previous works on ice matrices [38, 45–48]). All these considerations strengthen the idea of a necessary complete theoretical treatment (including thermal, optical, and in-plume aspects). Realizing this simulation on a molecular-level model seems almost impossible at the moment, due to the large timescales involved. The best results in this field (see [128] for a recent review) are still at the ps scale. However, a comprehensive macroscopic finite-elements approach could be very useful in better understanding the PAH sample evolution [41] under laser irradiation.

5.4.2. Wavelength-selective desorption versus ablation. The interpretation of the wavelength-selective desorption phenomenon observed on binary mixtures [40, 47] is somehow more complicated. The selective behaviour evidenced suggests a non-thermal mechanism. The non-thermal (or photochemical) desorption is evoked [105] in cases where the equilibration of energy is incomplete at the time of desorption. On the other hand, vibrational energy relaxation in condensed phases is known to be ultrafast [129–133] and the infrared resonant desorption may be expected to proceed via a thermal mechanism in which rapid vibrational relaxation would lead to heating of the sample and subsequent thermal desorption. However, theoretical studies [134–143] have predicted various non-thermal mechanisms where vibrational excitation of an adsorbate can promote desorption before the energy has thermalized. In a non-thermal process, only those adsorbates that were vibrationally excited initially would be desorbed, while co-adsorbates which were not excited would remain on the surface.

The presence of non-thermal mechanisms usually associated with the fast component of the velocity distribution has been claimed by several authors [65, 103–105, 144], but the precise nature of the physical processes involved could (generally) not be readily established. In this frame, resonant excitation is an intriguing possibility for the non-Boltzmann desorption channel [103, 144]. Burgess *et al* [103] studied the wavelength-dependence of the non-thermal desorption of NO adsorbed on platinum foil with 532 and 1064 nm lasers, but a negative result was obtained. In contrast, Hoheisel *et al* [144] claimed that the ejection of neutral atoms from small metal particles when a surface-plasmon oscillation is excited with laser light exhibits a strong resonant character and a non-thermal underlying mechanism. Moreover, in their C–H desorption study, Tro *et al* [39] depicted the 'ideal' IR laser desorption experiment for the evidence of the non-thermal single-photon resonant mechanism. However, their result on butane adsorbed on $Al_2O_3(11\bar{2}0)$ was negative: a thermal mechanism was observed, with quick thermalization of the vibration energy deposited in the C–H stretching mode.

Hussla *et al* [43] investigated the isotopically selective desorption of a NH_3:ND_3 (1:1) mixture adsorbed on Cu(100) or Ag film by resonant excitation of NH_3 in the 3 μm region. The result was negative, i.e., although only NH_3 molecules were initially excited by the IR photons, the co-adsorbed ND_3 desorbed with (almost) equal probability as NH_3, either by direct vibrational energy transfer or by thermally assisted processes. Previous work by Chuang [13, 14] on C_5H_5N and C_5D_5N co-adsorbed on KCl and excited by a CO_2 laser also showed lack of isotopic selectivity in the multi-photon excited desorption. Despite these negative results, Hussla *et al* [43] draw some general recommendations for suitable experimental systems and claim that 'one might be able ... to selectively desorb particular isotope species'.

Hess and co-workers [107, 145–148] reported in a series of papers on the UV photo-induced hyper-thermal halogen atom desorption from alkali halide surfaces and demonstrated that the yield, electronic state and velocity distributions of desorbed atoms can be controlled by careful choice of laser photon energy and pulse energy. The desorption is induced by the creation and decomposition of localized surface excitons, which can be viewed as a hole localized on a halogen atom and an excited electron loosely bound to the surface.

Natzle *et al* [105] evidenced in their study on the UV photodesorption of NO from condensed films that only the fast peak of the velocity distribution was present at low laser fluences, while at higher desorption yields the slow peaks also appeared. Moreover (see figure 7 of [105]), the fast peak (non-thermal) exhibited a linear fluence dependence, while the slow peak (thermal) displayed a clearly non-linear evolution. Some possible mechanisms have been listed for the non-thermal fast peak interpretation, but no definitive choice has been made.

These results present a strong similarity with our observations, and the attribution of the selective desorption regime to the fast peak of the velocity distribution is tempting. However,

more systematic measurements on the velocity distributions in this regime are needed in order to get a clear picture of the physical processes involved [40, 47].

6. Analytical and technological potential

6.1. LRD depth-profiling

The use of the laser resonant desorption mediated by the O–H stretching for the study of diffusion profiles of atmospheric interest trace gases into ice has been proposed by George's group [3]. Practically, the doped ice sample is layer-by-layer desorbed with consecutive laser shots and the dopant concentration is measured at each shot to draw the diffusion profile and derive the diffusion coefficient D. The main advantage of this technique on the previously used ones (e.g., serial mechanical cut followed by chromatographic analysis [149, 150]) is the excellent (in-depth) spatial resolution (sub-micrometric), which allows a diffusion time of several minutes, while the 25 μm resolution of the mechanical method needed diffusion times of at least four weeks.

Using this technique, George and co-workers measured diffusion profiles of HCl into ice at $T = 169$–195 K [3, 4, 29]. Later on, the diffusion coefficients of NH_3 (at $T \sim 140$ K) and CH_3OH (at $T = 169$–185 K) were measured [30]; some attempts have been made on the diffusion of SO_2 and C_4H_{10} into the ice, but this cannot be detected [30]. However, the use of this method for the measure of diffusion profiles has been criticized by Dominé and Xueref [151], who pointed out that the diffusion coefficients measured by Livingston *et al* [3] for HCl were several orders of magnitudes higher than the expected or measured values obtained by other techniques [149, 152] in the temperature range considered. Several possible problems have been suggested, at the level of the sample preparation or on the laser–solid thermal interaction itself. Preliminary work in our group tends to validate the hypothesis of Dominé and Xuéref [151]. Further work is needed to completely elucidate the possible dopant diffusion induced by thermal effects on the laser desorption timescale. An interesting perspective is to use a fs laser equipped with an IR OPA/DFG module (recently available in our laboratory) for the resonant desorption of ice-based samples on a much shorter timescale.

The C–H mode could offer the same opportunity for, for example, analysis of successive layers of soot deposits, although the penetration depth should be larger in this case, as mentioned above. A very interesting study has been recently reported on the depth-profiling of oleic acid adsorbed on glycerol aerosols by using a tunable IR OPO [153]. An intriguing selective desorption of the glycerol core has been evidenced when tuning the OPO in resonance with the O–H mode (instead of C–H, used for depth profiling); this behaviour has been tentatively explained by a 'shattering' effect.

The potentialities listed above, along with experimental facts not yet completely understood, illustrate the urgent need for a thorough characterization of the C–H promoted photodesorption process, especially in terms of spatial resolution achievable and/or its evolution with the laser fluence, which could be done for example by working on thin films of known thickness.

6.2. IR-MALDI

Since its introduction in the mid-1980s [1, 2], the MALDI technique has been usually associated with pulsed UV lasers. However, as early as 1990/1991, Overberg *et al* demonstrated the feasibility of the technique with IR pulsed sources, using first an Er:YAG laser at 2.94 μm [154] and shortly after a CO_2 laser at 10.6 μm [155]. Later on, the availability

of tunable IR OPOs and FELs led to an increased number of studies, most of them testing the performances of different potential matrices (see [28] for a recent review) and mainly in the 3 μm (O–H, C–H, N–H stretchings) and 6 μm (C = O stretching) spectral ranges. More recently, the overtone region (1.45–2 μm) has started to gain special interest (due to the potential use of high-power laser diodes as irradiation sources), but the results to date are negative [18] or of poor quality [25].

This plethora of studies is justified by some possible benefits of the IR-MALDI with respect to the UV variant. First of all, a wide range of potential matrices (with strong absorption near 3 μm) is available. In contrast to the almost exclusively strongly acidic UV matrices, several of the IR matrices with good performance (e.g., glycerol or tris/HCl) provide a more physiological environment for the analytes. One promising material is ice (though its performance as an IR matrix has not been fully proven [16, 25]), which would appear to be the natural matrix for biological molecules. Moreover, a water/glycerol mixture exhibited good qualities in this field [22, 24]. Another advantage of the IR-MALDI technique is the possibility to analyse photosensitive analytes with strong UV absorption. Finally, the IR-MALDI is now generally recognized as being a much softer desorption/ionization technique, compared to the UV variant [28], and also as leading to a particularly low degree of metastable ion fragmentation.

In spite of all these obvious advantages, the wide-scale implementation of the MALDI technique in IR is still limited compared to the UV domain. This could be due to the fact that the fundamentals of the IR technique in terms of desorption/ionization mechanisms, or even energy coupling itself, are not as well understood [25, 28] as for the UV approach [6]. Fundamental investigations starting with simple systems such as those presented above may thus bring a useful contribution in this field.

6.3. Pulsed laser cleaning

The wavelength-selective desorption observed in our studies recalls a model of thermo-elastic expansion usually employed in dry laser cleaning (DLC) to explain the removal of sub-micron particles from a surface without affecting the substrate [156]. In this model, the temperature rise induced by the absorbed light leads to a very small substrate expansion, which (considering the ns timescale of the process) results in high acceleration and ejection of the extraneous particles.

Since its introduction in 1991 [157] the pulsed laser cleaning technique has largely proven its efficiency in contaminant removal and consequently spreads its applications in a wide variety of fields, from nuclear decontamination [158] to integrated circuit manufacturing [159] or to restoration of cultural heritage [160]. The main concern of these technological developments has been to avoid (as far as possible) the substrate damage while selectively removing the undesirable contaminants (this is especially important for artwork conservation and restoration).

In our case the observed selective desorption could occur not only from the surface, but also from a small volume located under the surface. For instance, the penetration depth for one laser shot is about 0.3 μm at $\lambda \sim 3.1$ μm [38] and even higher at $\lambda \sim 3.3$ μm, if we consider the optical absorption coefficients for O–H and C–H modes [63]. A significant decrease in the overall signal has been observed after several hundred shots: this leads to a possibly affected depth of 10–100 μm. This 'volume' effect could be made possible by the high defect-density ice matrices (frozen solutions) employed [47].

The practical potential of the selective desorption technique has been demonstrated in our VIS/IR study [47] by cleaning of a 'dirty' ice surface contaminated with combustion soot particles (see figure 5 of [47]). While the technological interest is clearly established,

a thorough characterization of the optimum laser–sample interaction parameters (wavelength, fluence, pulse duration, etc) with respect to the contamination material and its specific relationship to the substrate is nevertheless necessary for a controlled wide-scale application.

6.4. Selective analysis of complex samples

From an analytical perspective, the wavelength-dependent effect evidenced above could be used in the selective analysis of complex samples. One example is the mixture of PAHs naturally present as adsorbed phase on combustion soot particles [161–169]. The specific shapes of the absorption bands corresponding to different PAHs turn into 'spectral signatures' by recording the desorption yield evolution when scanning the OPO idler wavelength across the C–H stretching mode range. Although not presented here, this selectivity at the desorption level could be especially interesting for the discrimination between isomers, when the mass resolution of the spectrometer employed is not enough to separate them. Sometimes this separation can be addressed at the ionization level by use of the REMPI (resonance enhanced multi-photon ionization) technique. However, several works pointed out the limitations of the REMPI technique when working with PAHs, especially concerning the loss of the selectivity in a one [170] or even two colour [171, 172] ionization scheme, due essentially to spectral congestion for large molecules and to the relative cross sections of the $S_1 \leftarrow S_0$ versus $IC \leftarrow S_1$ transitions (IC stands for ionization continuum). Such complications suggest that the REMPI technique alone could fail in the fine analysis of complex samples. The wavelength selectivity at the desorption level or the parametric selectivity on laser pulse energy demonstrated in a very recent study [51] could therefore constitute very useful allies in a combined approach for a complete determination of, for example, the composition of natural samples.

7. Conclusion

We report an overview of our recent laser resonant desorption studies in the 3 μm spectral range, using a pulsed tunable mid-infrared optical parametric oscillator. The resonant character of the desorption process of, respectively, pure ice, PAH and ammonia samples by excitation of the O–H ($\lambda = 3.1$ μm), C–H (3.3 μm) and N–H (2.9 μm) stretching modes has been investigated. An excellent agreement between the desorption yield and the corresponding absorption spectrum is obtained in the case of the O–H and C–H modes. This resonant character has been employed to desorb several cryogenic binary mixtures. In every case, a wavelength-selective effect has been found by comparative IR/IR or IR/visible irradiation studies. Indeed, highly preferential desorption of H_2O molecules is observed when in resonance with the O–H mode, in contrast with desorption of (almost exclusively) PAH molecules in the C–H stretching spectral region or with desorption of various metal salts at 532 nm, where they present a significant absorption coefficient. An increasing of the laser fluence and/or analyte concentration led to a loss of selectivity with co-desorption of both components. Thus, by choosing the adequate wavelength and laser fluence, one can control the desorption products. In certain cases, this loss of selectivity is accompanied by extensive hydrated cluster generation, which could have an important atmospherical (formaldehyde hydrated complexes) or biological (tryptophan–water clusters) interest.

The desorption plume dynamics has been probed in order to give some insights of the desorption mechanism. Surprisingly, the picture varies depending on whether the O–H or the C–H stretching mode is excited. In the first case, no signal has ever been observed after few hundred μs, while one can evidence the presence of desorbed PAHs 50 ms after the laser shots. This difference is tentatively explained in terms of thermal properties of the PAH samples and low optical absorption strength of the C–H mode.

Some possible explanations of the wavelength-selective phenomenon discovered have been outlined with respect to non-thermal mechanisms. However, a definite conclusion has not been reached. In this frame, the use of a fs laser equipped with an IR OPA/DFG module tunable up to 10 μm (recently available in our laboratory) provides an interesting perspective to probe the resonant non-thermal mechanisms on a much shorter timescale. This would also offer the opportunity to compare experimental results with available molecular dynamics simulations.

Possible applications of the LRD technique have been discussed in several directions, such as the IR-MALDI, the removal of a contaminant from a surface without affecting the substrate, the selective analysis of complex samples (possibly in combination with the REMPI technique and/or a parametric study on laser pulse energy) and the depth profiling of laboratory samples for trace gas diffusion.

Acknowledgments

The Centre d'Etudes et de Recherches Lasers et Applications is supported by the Ministère chargé de la Recherche, the Région Nord-Pas de Calais and the Fonds Européen de Développement Economique des Régions.

References

[1] Karas M, Bachmann D and Hillenkamp F 1985 *Anal. Chem.* **57** 2935
[2] Karas M, Bachmann D, Bahr U and Hillenkamp F 1987 *Int. J. Mass Spectrom. Ion Process.* **78** 53
[3] Livingston F E, Smith J A and George S M 2000 *Anal. Chem.* **72** 5590
[4] Livingston F E and George S M 2001 *J. Phys. Chem.* A **105** 5155
[5] Chrisey D B, Piqué A, McGill R A, Horwitz J S, Ringeisen B R, Bubb D M and Wu P K 2003 *Chem. Rev.* **103** 553
[6] Dreisewerd K 2003 *Chem. Rev.* **103** 395
[7] Georgiou S and Koubenakis A 2003 *Chem. Rev.* **103** 349
[8] Heidberg J, Stein H and Reihl E 1982 *Phys. Rev. Lett.* **49** 666
[9] Heidberg J, Stein H and Reihl E 1983 *Surf. Sci.* **126** 183
[10] Chuang T J 1982 *J. Chem. Phys.* **76** 3828
[11] Chuang T J and Seki H 1982 *Phys. Rev. Lett.* **49** 382
[12] Seki H and Chuang T J 1982 *Solid State Commun.* **44** 473
[13] Chuang T J 1983 *J. Electron Spectrosc. Relat. Phenom.* **29** 125
[14] Chuang T J 1983 *Surf. Sci. Rep.* **3** 1
[15] Cramer R, Hillenkamp F and Haglund R F Jr 1996 *J. Am. Soc. Mass Spectrom.* **7** 1187
[16] Berkenkamp S, Karas M and Hillenkamp F 1996 *Proc. Natl Acad. Sci. USA* **93** 7003
[17] Cramer R, Haglund R F Jr and Hillenkamp F 1997 *J. Mass Spectrom. Ion Process.* **169/170** 51
[18] Caldwell K L, McGarity D R and Murray K K 1997 *J. Mass Spectrom.* **32** 1374
[19] Sadeghi M, Olumee Z, Tang X, Vertes A, Jiang Z X, Henderson A J, Sang Lee H and Prasad C R 1997 *Rapid Commun. Mass Spectrom.* **11** 393
[20] Berkenkamp S, Menzel C, Karas M and Hillenkamp F 1997 *Rapid Commun. Mass Spectrom.* **11** 1399
[21] Hess W P, Park H K, Yavas O and Haglund R F Jr 1998 *Appl. Surf. Sci.* **127–129** 235
[22] Caldwell K L and Murray K K 1998 *Appl. Surf. Sci.* **127–129** 242
[23] Sheffer J D and Murray K K 1998 *Rapid Commun. Mass Spectrom.* **12** 1685
[24] Kraft P, Alimpiev S, Dratz E and Sunner J 1998 *J. Am. Soc. Mass Spectrom.* **9** 912
[25] Menzel C, Dreisewerd K, Berkenkamp S and Hillenkamp F 2001 *Int. J. Mass Spectrom.* **207** 73
[26] Laiko V V, Taranenko N I, Berkout V D, Yakshin M A, Prasad C R, Sang Lee H and Doroshenko V M 2002 *J. Am. Soc. Mass Spectrom.* **13** 354
[27] Baltz-Knorr M L, Scriver K E and Haglund R F 2002 *Appl. Surf. Sci.* **197/198** 11
[28] Dreisewerd K, Berkenkamp S, Leisner A, Rohlfing A and Menzel C 2003 *Int. J. Mass Spectrom.* **226** 189
[29] Livingston F E and George S M 2002 *J. Phys. Chem.* A **106** 5114
[30] Livingston F E, Smith J A and George S M 2002 *J. Phys. Chem.* A **106** 6309
[31] Yavas O, Maddocks E L, Papantonakis M R and Haglund R F Jr 1998 *Appl. Surf. Sci.* **127–129** 26

[32] Ermer D R, Papantonakis M R, Baltz-Knorr M, Nakazawa D and Haglund R F Jr 2000 *Appl. Phys.* A **70** 633
[33] Sturmann J, Albridge R G, Barnes A V, Davidson J L, Gilligan J M, Lüpke G, Ueda A and Tolk N H 1998 *Appl. Surf. Sci.* **127–129** 59
[34] Bubb D M, Horwitz J S, McGill R A, Chrisey D B, Papantonakis M R, Haglund R F Jr and Toftmann B 2001 *Appl. Phys. Lett.* **79** 2847
[35] Walsh J T Jr, Flotte T J and Deutsch T F 1989 *Lasers Surg. Med.* **9** 314
[36] Walsh J T Jr and Deutsch T F 1989 *Lasers Surg. Med.* **9** 327
[37] Krasnopoler A and George S M 1998 *J. Phys. Chem.* B **102** 788
[38] Focsa C, Chazallon B and Destombes J L 2003 *Surf. Sci.* **528** 189
[39] Tro N J, Arthur D A and George S M 1989 *J. Chem. Phys.* **90** 3389
[40] Mihesan C, Ziskind M, Chazallon B, Therssen E, Desgroux P, Gurlui S and Focsa C 2005 *Appl. Surf. Sci.* at press
[41] Mihesan C, Ziskind M, Therssen E, Desgroux P and Focsa C 2005 *Chem. Phys. Lett.* submitted
[42] Chuang T J and Hussla I 1984 *Phys. Rev. Lett.* **52** 2045
[43] Hussla I, Seki H, Chuang T J, Gortel Z W, Kreuzer H J and Piercy P 1985 *Phys. Rev.* B **32** 3489
[44] Redlich B, Zacharias H, Meijer G and von Helden G 2002 *Surf. Sci.* **502/503** 325
[45] Ziskind M, Mihesan C, Lebrun N, Chazallon B, Focsa C and Destombes J L 2004 *Appl. Phys.* A **79** 991
[46] Mihesan C, Lebrun N, Ziskind M, Chazallon B, Focsa C and Destombes J L 2004 *Surf. Sci.* **566–568** 650
[47] Mihesan C, Ziskind M, Chazallon B, Therssen E, Desgroux P and Focsa C 2005 *Surf. Sci.* **593** 221
[48] Mihesan C, Ziskind M, Chazallon B, Focsa C and Destombes J L 2005 *Appl. Surf. Sci.* **248** 238
[49] Focsa C and Destombes J L 2001 *Chem. Phys. Lett* **347** 390
[50] Mihesan C, Gurlui S, Ziskind M, Chazallon B, Martinelli G, Zeghlache H, Guignard M, Nazabal V, Smektala F and Focsa C 2005 *Appl. Surf. Sci.* **248** 224
[51] Mihesan C, Ziskind M, Therssen E, Desgroux P and Focsa C 2005 *J. Phys. Conf. Ser.* submitted
[52] Petrenko V F and Whitworth R W 1999 *Physics of Ice* (Oxford: Oxford University Press)
[53] Khusnatdinov N N and Petrenko V F 1996 *J. Cryst. Growth* **163** 420
[54] Solomon S 1988 *Rev. Geophys.* **26** 132
[55] Hobbs P V 1974 *Ice Physics* (Oxford: Clarendon)
[56] Irvine W M and Pollack J B 1968 *Icarus* **8** 324
[57] Bertie J E, Labbé H J and Whalley E 1969 *J. Chem. Phys.* **50** 4501
[58] Vodopyanov K L 1991 *J. Chem. Phys.* **94** 5389
[59] Cummings J P and Walsh J T Jr 1993 *Appl. Phys. Lett.* **62** 1988
[60] Toon O B, Tolbert M A, Koehler B G, Middlebrook A and Jordan J 1994 *J. Geophys. Res.* **99** 25631
[61] Coblentz Society, Inc. 2005 Evaluated infrared reference spectra *NIST Chemistry WebBook Standard Reference Database No. 69* ed P J Linstrom and W G Mallard (Gaithersburg MD: National Institute of Standards and Technology) p 20899 (http://webbook.nist.gov)
[62] d'Hendecourt L B and Allamandola L J 1986 *Astron. Astrophys. Suppl. Ser.* **64** 453
[63] Sandford S A, Bernstein M P and Allamandola L J 2004 *Astrophys. J.* **607** 346
[64] Yingling Y G, Zhigilei L V, Garrison B J, Koubenakis A, Labrakis J and Georgiou S 2001 *Appl. Phys. Lett.* **78** 1631
[65] Koubenakis A, Elimioti T and Georgiou S 1999 *Appl. Phys.* A **69** S637
[66] Dreisewerd K, Schürenberg M, Karas M and Hillenkamp F 1995 *Int. J. Mass Spectrom. Ion Process.* **141** 127
[67] Zhigilei L V and Garrison B J 2000 *J. Appl. Phys.* **88** 1281
[68] Zhigilei L V and Garrison B J 1999 *Appl. Phys. Lett.* **74** 1341
[69] Zhigilei L V, Kodali P B S and Garrison B J 1997 *Chem. Phys. Lett.* **276** 269
[70] Lebrun N, Dhamelincourt P, Focsa C, Chazallon B, Destombes J L and Prevost D 2003 *J. Raman Spectrosc.* **34** 459
[71] Chazallon B, Lebrun N, Dhamelincourt P, Toubin C and Focsa C 2005 *J. Phys. Chem.* B **109** 432
[72] Katz R N, Chaudhary T and Field F H 1986 *J. Am. Chem. Soc.* **108** 3897
[73] Kosevich M V, Czira G, Boryak O A, Shelkovsky V S and Vékey K 1997 *Rapid Commun. Mass Spectrom.* **11** 1411
[74] Boryak O A, Kosevich M V and Shelkovsky V S 1997 *Int. J. Mass Spectrom. Ion Process.* **163** 177
[75] Kosevich M V 1997 *Eur. J. Mass Spectrom.* **3** 320
[76] Kosevich M V, Czira G, Boryak O A, Shelkovsky V S and Vékey K 1998 *J. Mass Spectrom.* **33** 843
[77] Sunner J, Ikonomou M G and Kebarle P 1988 *Int. J. Mass Spectrom. Ion Process.* **82** 221
[78] Snoek L C, Kroemer R T, Hockridge M R and Simons J P 2001 *Phys. Chem. Chem. Phys.* **3** 1819
[79] Philips L A, Webb S P, Martinez S J III, Fleming G R and Levy D H 1988 *J. Am. Chem. Soc.* **110** 1352
[80] Rizzo T R, Park Y D, Peteanu L A and Levy D H 1986 *J. Chem. Phys.* **84** 2534

[81] Piuzzi F, Dimicoli I, Mons M, Tardivel B and Zhao Q 2000 *Chem. Phys. Lett.* **320** 282
[82] Snoek L C, Kroemer R T and Simons J P 2002 *Phys. Chem. Chem. Phys.* **4** 2130
[83] Cable J R, Tubergen M J and Levy D H 1989 *J. Am. Chem. Soc.* **111** 9032
[84] Belov M E, Alimpiev S S, Mlynsky V V, Nikiforov S M and Derrick P J 1995 *Rapid Commun. Mass Spectrom.* **9** 1431
[85] Zhan Q, Wright S J and Zenobi R 1997 *J. Am. Soc. Mass Spectrom.* **8** 525
[86] Peteanu L A and Levy D H 1988 *J. Phys. Chem.* **92** 6554
[87] Mons M, Dimicoli I, Tardivel B, Piuzzi F, Brenner V and Millié P 1999 *J. Phys. Chem.* A **103** 9958
[88] Boryak O A, Stepanov I O, Kosevich M V, Shelkovsky V S, Orlov V V and Blagoy Y P 1996 *Eur. Mass. Spectrom.* **2** 329
[89] Boryak O A, Kosevich M V, Shelkovsky V S and Blagoy Y P 1996 *Rapid Commun. Mass. Spectrom.* **10** 197
[90] Sobott F, Wattenberg A, Barth H-D and Brutschy B 1999 *Int. J. Mass Spectrom.* **185–187** 271
[91] Handschuh M, Nettesheim S and Zenobi R 1999 *Appl. Surf. Sci.* **137** 125
[92] Pocsik I 1991 *Z. Phys.* D **20** 395
[93] Wang C R, Huang R B, Liu Z Y and Zheng L S 1994 *Chem. Phys. Lett.* **227** 103
[94] Björneholm O, Federmann F, Kakar S and Möller T 1999 *J. Chem. Phys.* **111** 546
[95] Miyazaki M, Fujii A, Ebata T and Mikami N 2004 *Science* **304** 1134
[96] Shin J-W, Hammer N I, Diken E G, Johnson M A, Walters R S, Jaeger T D, Duncan M A, Christie R A and Jordan K D 2004 *Science* **304** 1137
[97] Miyazaki M, Fujii A, Ebata T and Mikami N 2004 *J. Phys Chem.* A **108** 10656
[98] Guillaume C, Le Calvé J, Dimicoli I and Mons M 1994 *Z. Phys.* D **32** 157
[99] Courty A, Mons M, Le Calvé J, Piuzzi F and Dimicoli I 1997 *J. Phys. Chem.* A **101** 1445
[100] Glückmann M and Karas M 1999 *J. Mass Spectrom.* **226** 239
[101] Karas M, Bahr U, Fournier I, Glückmann M and Pfenninger A 2003 *Int. J. Mass. Spectrom.* **226** 239
[102] Karas M and Krüger R 2003 *Chem. Rev.* **103** 427
[103] Burgess D Jr, Cavanagh R R and King D S 1988 *J. Chem. Phys.* **88** 6556
[104] Budde F, Hamza A V, Ferm P M, Ertl G, Weide D, Andresen P and Freund H J 1988 *Phys. Rev. Lett.* **60** 1518
[105] Natzle W C, Padowitz D and Sibener S J 1988 *J. Chem. Phys.* **88** 7975
[106] Cousins L M, Levis R J and Leone S R 1989 *J. Chem. Phys.* **91** 5731
[107] Hess W P, Joly A G, Gerrity D P, Beck K M, Sushko P V and Shluger A L 2001 *J. Chem. Phys.* **115** 9463
[108] Beck K M, Joly A G and Hess W P 2001 *Phys. Rev.* B **63** 125423
[109] Domen K and Chuang T J 1989 *J. Chem. Phys.* **90** 3318
[110] Domen K and Chuang T J 1989 *J. Chem. Phys.* **90** 3332
[111] Beavis R C and Chait B T 1991 *Chem. Phys. Lett.* **181** 479
[112] Estler R C and Nogar N S 1991 *J. Appl. Phys.* **69** 1654
[113] Zhigilei L V and Garrison B J 1998 *Rapid Commun. Mass Spectrom.* **12** 1273
[114] Williams G J, Zhigilei L V and Garrison B J 2001 *Nucl. Instrum. Methods* B **180** 209
[115] Kools J C S, Baller T S, De Zwart S T and Dieleman J 1992 *J. Appl. Phys.* **71** 4547
[116] Kelly R and Dreyfus R W 1988 *Nucl. Instrum. Methods* B **32** 341
[117] Kelly R and Dreyfus R W 1988 *Surf. Sci.* **198** 263
[118] Kelly R 1990 *J. Chem. Phys.* **92** 5047
[119] Kelly R 1990 *Nucl. Instrum. Methods* B **46** 441
[120] Kelly R 1992 *Phys. Rev.* A **46** 860
[121] Kelly R, Miotello A, Braren B, Gupta A and Casey K 1992 *Nucl. Instrum. Methods* B **65** 187
[122] Miotello A and Kelly R 1995 *Appl. Phys. Lett.* **67** 3535
[123] Kelly R and Miotello A 1997 *Nucl. Instrum. Methods* B **122** 374
[124] Kelly R and Miotello A 1999 *Phys. Rev.* E **60** 2616
[125] Anderson J B 1974 *Molecular Beams and Low Density Gas Dynamics* ed P P Wegener (New York: Dekker)
[126] Takamizawa A, Kajimoto S, Hobley J, Hatanaka K, Ohta K and Fukumura H 2003 *Phys. Chem. Chem. Phys.* **5** 888
[127] Zhigilei L V 2003 *Appl. Phys.* A **76** 339
[128] Zhigilei L V, Leveugle E, Garrison B J, Yingling Y G and Zeifman M I 2003 *Chem. Rev.* **103** 321
[129] Laubereau A and Kaiser W 1978 *Rev. Mod. Phys.* **50** 607
[130] Laubereau A, Fischer S F, Spanner K and Kaiser W 1978 *Chem. Phys.* **31** 335
[131] Fendt A, Fischer S F and Kaiser W 1981 *Chem. Phys.* **57** 55
[132] Heilweil E J, Casassa M P, Cavanagh R R and Stephenson J C 1985 *Chem. Phys.* **82** 5216
[133] Heilweil E J 1986 *Chem. Phys. Lett.* **129** 48
[134] Lin J and George T F 1980 *J. Chem. Phys.* **72** 2554

[135] Lin J and George T F 1980 *J. Phys. Chem.* **84** 2957
[136] Lucas D and Ewing G E 1981 *Chem. Phys.* **58** 385
[137] Kreuzer H J and Lowy D N 1981 *Chem. Phys. Lett.* **78** 50
[138] Gortel Z W, Kreuzer H J, Piercy P and Teshima R 1983 *Phys. Rev.* B **27** 5066
[139] Gortel Z W, Kreuzer H J, Piercy P and Teshima R 1983 *Phys. Rev.* B **28** 2119
[140] Cellii F G, Casassa M P and Janda K 1984 *Surf. Sci.* **141** 169
[141] Fain B and Lin S H 1985 *Chem. Phys. Lett.* **114** 497
[142] Gortel Z W, Piercy P, Teshima R and Kreuzer H J 1986 *Surf. Sci.* **165** L12
[143] Gortel Z W, Piercy P, Teshima R and Kreuzer H J 1987 *Surf. Sci.* **179** 176
[144] Hoheisel W, Jungmann K, Vollmer M, Weidenauer R and Träger F 1988 *Phys. Rev. Lett.* **60** 1649
[145] Hess W P, Joly A G, Gerrity D P, Beck K M, Sushko P V and Shluger A L 2002 *J. Chem. Phys.* **116** 8144
[146] Joly A G, Beck K M, Henyk M, Hess W P, Sushko P V and Shluger A L 2003 *Surf. Sci.* **544** L683
[147] Beck K M, Joly A G, Dupuis N F, Perozzo P, Hess W P, Sushko P V and Shluger A L 2004 *J. Chem. Phys.* **120** 2456
[148] Hess W P, Joly A G, Beck K M, Sushko P V and Shluger A L 2004 *Surf. Sci.* **564** 62
[149] Thibert E and Dominé F 1997 *J. Phys. Chem.* B **101** 3554
[150] Thibert E and Dominé F 1998 *J. Phys. Chem.* B **102** 4432
[151] Dominé F and Xueref I 2001 *Anal. Chem.* **73** 4348
[152] Fluckiger B, Chaix L and Rossi M J 2000 *J. Phys. Chem.* A **104** 11739
[153] Woods E III, Smith G D, Miller R E and Baer T 2002 *Anal. Chem.* **74** 1642
[154] Overberg A, Karas M, Bahr U, Kaufmann R and Hillenkamp F 1990 *Rapid Commun. Mass Spectrom.* **4** 293
[155] Overberg A, Karas M and Hillenkamp F 1991 *Rapid Commun. Mass Spectrom.* **5** 128
[156] Arnold N 2002 *Laser Cleaning* vol 51, ed B Lukiyanchuk (Singapore: World Scientific)
[157] Zapka W, Ziemlich W and Tam A C 1991 *Appl. Phys. Lett.* **58** 2217
[158] Delaporte Ph, Gastaud M, Marine W, Sentis M, Uteza O, Thouvenot P, Alcaraz J L, Le Samedy J M and Blin D 2003 *Appl. Surf. Sci.* **208/209** 298
[159] Lu Y F, Zheng Y W and Song W D 2000 *J. Appl. Phys.* **87** 1534
[160] Kautek W, Pentzien S, Krüger J and König E 1997 Lasers in the conservation of artworks I *Restauratorenblätter* ed W Kautek and E König (Wien: Mayer & Comp.) (Special Issue)
[161] Hankin S M and John P 1999 *Anal. Chem.* **71** 1100
[162] Marr L C, Kirchstetter T W, Harley R A, Miguel A H, Hering S V and Hammond S K 1999 *Environ. Sci. Technol.* **33** 3091
[163] Leotz-Gartziandia E, Tatry V and Carlier P 2000 *Polycyclic Aromatic Compounds* **20** 245
[164] Zimmermann R, Van Vaeck L, Davidovic M, Beckmann M and Adams F 2000 *Environ. Sci. Technol.* **34** 4780
[165] Carré V, Vernex-Loset L, Krier G, Manuelli P and Muller J-F 2004 *Anal. Chem.* **76** 3979
[166] Dobbins R A, Fletcher R A and Lu W 1995 *Combust. Flame* **100** 301
[167] Dobbins R A, Fletcher R A and Chang H-C 1998 *Combust. Flame* **115** 285
[168] Öktem B, Tolocka M P and Johnston M V 2004 *Anal. Chem.* **76** 253
[169] Öktem B, Tolocka M P, Zhao B, Wang H and Johnston M V 2005 *Combust. Flame* **142** 364
[170] Haefliger O P and Zenobi R 1998 *Anal. Chem.* **70** 2660
[171] Hager J C and Wallace S C 1988 *Anal. Chem.* **60** 5
[172] Velasquez J, Volobоueva L A and Cool T A 1998 *Combust. Sci. Technol.* **134** 139